The Journal of Experimental Biology 208, 3785-3804
Published by The Company of Biologists 2005
doi:10.1242/jeb.01852

A computational study of the aerodynamics and forewing–hindwing interaction of a model dragonfly in forward flight

Ji Kang Wang and Mao Sun*

Ministry-of-Education Key Laboratory of Fluid Mechanics, Institute of Fluid Mechanics, Beijing University of Aeronautics and Astronautics, Beijing 100083, People's Republic of China

*Author for correspondence (e-mail: m.sun@263.net)

Accepted 12 August 2005

Summary

The aerodynamics and forewing–hindwing interaction of a model dragonfly in forward flight are studied, using the method of numerically solving the Navier–Stokes equations. Available morphological and stroke-kinematic parameters of dragonfly (*Aeshna juncea*) are used for the model dragonfly. Six advance ratios (*J*; ranging from 0 to 0.75) and, at each *J*, four forewing–hindwing phase angle differences (γ_d; 180°, 90°, 60° and 0°) are considered. The mean vertical force and thrust are made to balance the weight and body-drag, respectively, by adjusting the angles of attack of the wings, so that the flight could better approximate the real flight.

At hovering and low *J* (*J*=0, 0.15), the model dragonfly uses separated flows or leading-edge vortices (LEV) on both the fore- and hindwing downstrokes; at medium *J* (*J*=0.30, 0.45), it uses the LEV on the forewing downstroke and attached flow on the hindwing downstroke; at high *J* (*J*=0.6, 0.75), it uses attached flows on both fore- and hindwing downstrokes. (The upstrokes are very lightly loaded and, in general, the flows are attached.)

At a given *J*, at γ_d=180°, there are two vertical force peaks in a cycle, one in the first half of the cycle, produced mainly by the hindwing downstroke, and the other in the second half of the cycle, produced mainly by the forewing downstroke; at γ_d=90°, 60° and 0°, the two force peaks merge into one peak. The vertical force is close to the resultant aerodynamic force [because the thrust (or body-drag) is much smaller than vertical force (or the weight)]. 55–65% of the vertical force is contributed by the drag of the wings.

The forewing–hindwing interaction is detrimental to the vertical force (and resultant force) generation. At hovering, the interaction reduces the mean vertical force (and resultant force) by 8–15%, compared with that without interaction; as *J* increases, the reduction generally decreases (e.g. at *J*=0.6 and γ_d=90°, it becomes 1.6%). A possible reason for the detrimental interaction is as follows: each of the wings produces a mean vertical force coefficient close to half that needed for weight support, and a downward flow is generated in producing the vertical force; thus, in general, a wing moves in the downwash-velocity field induced by the other wing, reducing its aerodynamic forces.

Key words: dragonfly, forward flight, unsteady aerodynamics, forewing–hindwing interaction, Navier–Stokes simulation.

Introduction

Scientists have always been fascinated by the flight of dragonflies. Analysis based on quasi-steady aerodynamic theory has shown that the vertical force required for weight support is much greater than the steady-state values measured from dragonfly wings, suggesting that unsteady aerodynamics must play important roles in the flight of dragonflies (Norberg, 1975; Wakeling and Ellington, 1997a,b,c).

Force measurement on a tethered dragonfly was conducted by Somps and Luttges (1985). It was shown that over some part of a stroke cycle, vertical force was many times larger than the dragonfly weight. They considered that the large force might be due to the effect of forewing–hindwing interaction. Flow visualization studies on flapping model dragonfly wings were conducted by Saharon and Luttges (1988, 1989), and it was shown that constructive or destructive wing/flow interactions might occur, depending on the kinematic parameters of the flapping motion. In these studies, only the total force of the fore- and hindwings was measured and, moreover, force measurements and flow visualizations were conducted in separate works. Experimental (Freymuth, 1990) and computational (Wang, 2000) studies on an airfoil (two-dimensional wing) in dragonfly hovering mode showed that large vertical force was produced during each downstroke and that the mean vertical force was enough to support the weight of a typical dragonfly. During each downstroke, a vortex pair was created; the large vertical force was explained by the downward two-dimensional jet induced by the vortex pair (Wang, 2000). In these works (Freymuth, 1990; Wang, 2000), because only a single airfoil was used, the effects of interaction between the fore- and hindwings and the three-dimensional

flow effects could not be considered. Flow visualization studies on free-flying and tethered dragonflies were recently conducted by Thomas et al. (2004). It was shown that dragonflies fly by using unsteady aerodynamic mechanisms to generate leading-edge vortices (LEVs) or high lift when needed and that the dragonflies controlled the flow mainly by changing the angle of attack of the wings. Their results represent the only existing data on the flow around the wings of free-flying dragonflies.

Recently, Sun and Lan (2004) studied the aerodynamics and the forewing–hindwing interaction of the dragonfly *Aeshna juncea* in hover flight, using the method of computational fluid dynamics (CFD). Three-dimensional wings and wing kinematics data of free-flight were employed in the study. They showed that the vertical force coefficient of the forewing or the hindwing was twice as large as the quasi-steady value and that the mean vertical force could balance the dragonfly weight. They also showed that the large vertical force coefficient was due to the LEV associated with the delayed stall mechanism and that the interaction between the fore- and hindwings was not very strong and was detrimental to the vertical force generation. The result of detrimental interaction is interesting. But Sun and Lan (2004) investigated only a specific case of flight in *Aeshna juncea*, i.e. hovering with 180° phase difference between the fore- and hindwings. Whether the result that forewing–hindwing interaction is detrimental is a local result due to the specific kinematics used or is a more general result is not known. It is desirable to make further studies on dragonfly aerodynamics at various flight conditions and on the problem of forewing–hindwing interaction.

In the present study, we address the above questions by numerical simulation of the flows of a model dragonfly in forward flight. The vertical force and thrust are made to balance the insect weight and body-drag, respectively, by adjusting the angles of attack of the wings, so that the simulated flight could better approximate the real flight. The phasing and the incoming flow speed (flight speed) of the model dragonfly are systematically varied. At each flight speed, four phase differences –0°, 60°, 90° and 180° (the hindwing leads the forewing motion) – are considered. Dragonflies vary the phase difference between the fore- and hindwings with different behaviours (Norberg, 1975; Azuma and Watanabe, 1988; Reavis and Luttges, 1988; Wakeling and Ellington, 1997b; Wang et al., 2003; Thomas et al., 2004). It has been shown that a 55–100° phase difference (the hindwing leads forewing motion) is commonly used in straight forward flight (e.g. Azuma and Watanabe, 1988; Wang et al., 2004) and a 180° phase difference is used in hovering (e.g. Norberg, 1975). Recent observation by Thomas et al. (2004) has shown that 180° phase difference is also used in forward flight. We chose 60°, 90° and 180° to represent the above range of phase difference. Although 0° phase difference (parallel stroking) has been mainly found in accelerating or manoeuvring flight (e.g. Alexander, 1986; Thomas et al., 2004), this phase difference is also included for reference. As in Sun and Lan (2004), the approach of solving the flow equations over moving overset grids is employed because of the unique feature of the motion, i.e. the fore- and hindwings move relative to each other.

Materials and methods

The model wings

The model fore- and hindwings (Fig. 1) are the same as those used in Sun and Lan (2004). The thickness of the wings is 1% of c (where c is the mean chord length of the forewing). The planforms of the wings are similar to those of the wings of *Aeshna juncea* (Norberg, 1972). The fore- and hindwings are the same length, but the chord length of the hindwing is larger than that of the forewing. The radius of the second moment of the forewing area is denoted by r_2, and r_2=0.61R, where R is the wing length (the mean flapping velocity at r_2 is used as the reference velocity in the present study).

The flow computation method and evaluation of the aerodynamic forces

The flow equations and computational method used in the present study are the same as those used in Sun and Lan (2004). Only an outline of the method is given here. The Navier–Stokes equations are numerically solved using moving overset grids. The algorithm was first developed by Rogers and Kwak (1990) and Rogers et al. (1991) for single-grid, which

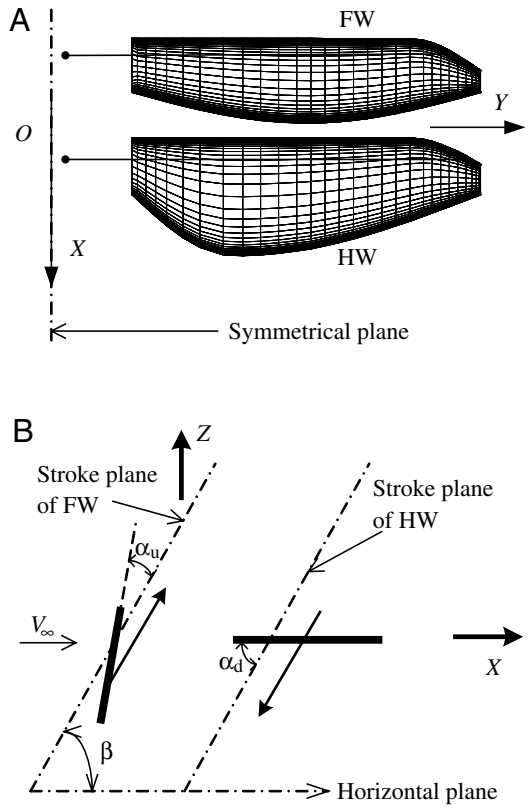

Fig. 1. Sketches of the model wings, the flapping motion and the reference frames. FW and HW denote fore- and hindwings, respectively. O,X,Y,Z is an inertial frame, with the X and Y axes in the horizontal plane. β, stroke plane angle; V_∞, incoming flow velocity.

is based on the method of artificial compressibility, and it was extended by Rogers and Pulliam (1994) to overset grids. The time derivatives of the momentum equations are differenced using a second-order, three-point backward difference formula. The derivatives of the viscous fluxes in the momentum equation are approximated using second-order central differences. For the derivatives of convective fluxes, upwind differencing based on the flux-difference splitting technique is used. A third-order upwind differencing is used at the interior points, and a second-order upwind differencing is used at points next to boundaries. With overset grids (Fig. 2), for each wing there is a body-fitted curvilinear grid, which extends a relatively short distance from the body surface, and in addition, there is a background Cartesian grid, which extends to the far-field boundary of the domain. The solution method for single-grid is applied to each of these grids; data are interpolated from one grid to another at the inter-grid boundary points.

Only the flow on the right of the plane of symmetry (Fig. 1A) is computed; the effects of left wings are taken into consideration by the central mirroring condition. The overset-grid system used here is the same as that in Sun and Lan (2004). Each of the wing grids had dimensions 29×77×45 in the normal direction, around the wing and in the spanwise direction, respectively, and the background grid had dimensions 46×94×72 in the *Y*-direction and directions parallel and normal to the stroke-planes, respectively. The time step value used ($\Delta\tau$=0.02) is also the same as that in Sun and Lan (2004).

In the present study, the lift of a wing is defined as the component of the aerodynamic force on the wing that is perpendicular to the translational velocity of the wing (i.e. perpendicular to the stroke plane), and the drag of a wing is defined as the component that is parallel to the translational velocity (note that these are not the conventional definitions of lift and drag; the conventional ones are the components of force perpendicular and parallel to the relative airflows, respectively). l_f and d_f denote the lift and drag of the forewing, respectively; l_h and d_h denote the lift and drag of the hindwing, respectively. Resolving the lift and drag into the Z and X axes gives the vertical force and thrust of a wing. V_f and T_f denote the vertical force and thrust of the forewing, respectively; V_h and T_h denote the vertical force and thrust of the hindwing, respectively. For the forewing:

$$V_f = l_f \cos\beta + d_f \sin\phi \sin\beta , \quad (1)$$

$$T_f = l_f \sin\beta - d_f \sin\phi \cos\beta . \quad (2)$$

These two formulae also apply to the hindwing. The coefficients of V_f, T_f, V_h, T_h, l_f, d_f, l_h and d_h are denoted as $C_{V,f}$, $C_{T,f}$, $C_{V,h}$, $C_{T,h}$, $C_{l,f}$, $C_{d,f}$, $C_{l,h}$ and $C_{d,h}$, respectively. They are defined as:

$$C_{V,f} = V_f / [0.5\rho U^2 (S_f + S_h)] , \text{ etc.}, \quad (3)$$

where ρ is the fluid density, S_f and S_h are the areas of the fore- and hindwings, respectively. The total vertical force (V) and total thrust (T) of the fore- and hindwings are V=V_f+V_h and T=T_f+T_h, respectively. The coefficients of V and T are denoted as C_V and C_T, respectively, and defined as:

$$C_V = V / [0.5\rho U^2 (S_f + S_h)] = C_{V,f} + C_{V,h} , \quad (4)$$

$$C_T = T / [0.5\rho U^2 (S_f + S_h)] = C_{T,f} + C_{T,h} . \quad (5)$$

Conventionally, reference velocity used in the definition of force coefficients of a wing is the relative velocity of the wing. In the above definition of force coefficients, U is used as the reference velocity. At hovering, U is the mean relative velocity of the wings. It should be noted that at forward flight, U is not the mean relative velocity of the wings and the above definition of force coefficients is different from the conventional one.

Kinematics of flapping wings

The flapping motions of the wings are shown in Fig. 1. The free-stream velocity, which has the same magnitude as the flight velocity, is denoted by V_∞, and the stroke plane angle is denoted by β (Fig. 1B). The azimuthal rotation of a wing is called 'translation', and the pitching (or flip) rotation of the wing near the end of a half-stroke and at the beginning of the following half-stroke is called rotation. The speed at r_2 is called the translational speed. The wing translates downwards and upwards along the stroke plane and rotates during stroke reversal (Fig. 1B). The translational velocity is denoted by u_t and is given by:

$$u_t^+ = 0.5\pi \sin(2\pi\tau/\tau_c + \gamma) , \quad (6)$$

where the non-dimensional translational velocity u_t^+=u_t/U (U is the reference velocity); the non-dimensional time τ=tU/c (t is the time; c is the mean chord length of the forewing, used as reference length in the present study); τ_c is the non-dimensional period of the flapping cycle; and γ is the phase angle of the translation of the wing. The reference velocity is U=$2\Phi n r_2$, where Φ and n are the stroke amplitude and stroke frequency of the forewing, respectively. Denoting the azimuth-rotational velocity as $\dot{\phi}$, we have $\dot{\phi}$=u_t/r_2. The geometric angle

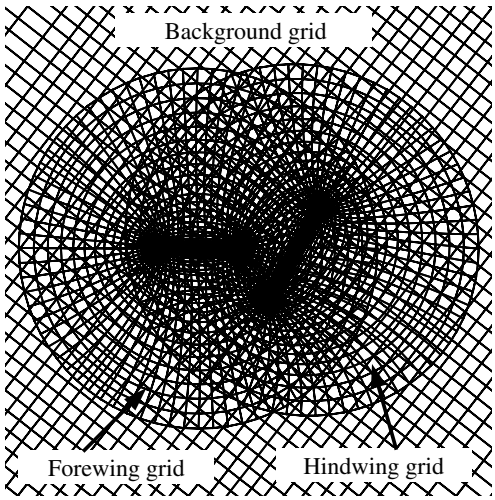

Fig. 2. Some portions of the moving overset grids.

attack of the wing is defined as the acute angle between the stroke plane and the wing-surface plane, which assumes a constant value during the translational portion of a half-stroke; the constant value is denoted by α_d for the downstroke and by α_u for the upstroke (Fig. 1). Around the stroke reversal, the angle of attack changes with time, and the angular velocity ($\dot{\alpha}$) is given by:

$$\dot{\alpha}^+ = 0.5\dot{\alpha}_0^+ \{1 - \cos [2\pi (\tau - \tau_r) / \Delta\tau_r]\} , \tau_r \leqslant \tau \leqslant \tau_r + \Delta\tau_r , \quad (7)$$

where the non-dimensional form $\dot{\alpha}^+=\dot{\alpha}c/U$; $\dot{\alpha}_0^+$ is a constant; τ_r is the time at which the rotation starts; and $\Delta\tau_r$ is the time interval over which the rotation lasts. In the time interval of $\Delta\tau_r$, the wing rotates from α_u to α_d. Therefore, when α_d, α_u and $\Delta\tau_r$ are specified, $\dot{\alpha}_0^+$ can be determined (around the next stroke reversal, the wing would rotate from α_u to α_d, and the sign of the right-hand side of Eqn 7 should be reversed). The axis of the flip rotation is located at a distance of 24% of the mean chord length of the wing from the leading edge. With U and c as the reference velocity and reference length, respectively, the Reynolds number (Re) is defined as $Re=Uc/\nu=2\Phi nr_2c/\nu$ (ν is the kinematic viscosity of the air), and the advance ratio (J) is defined as $J=V_\infty/2\Phi nR)=V_\infty/(UR/r_2)$.

Non-dimensional parameters of wing motion

In the flapping motion described above, we need to specify the flapping period (τ_c), the reference velocity (U), the geometrical angles of attack (α_d and α_u), the wing rotation duration ($\Delta\tau_r$), the phase difference (γ_d) between hindwing and forewing, the mean flapping angle ($\bar{\phi}$) and the stroke plane angle (β). For the flow computation, we also need to specify Re and J.

For the dragonfly *Aeshna juncea* in hovering flight, the following kinematic data are available (Norberg, 1975): $\beta\approx60°$, n=36 Hz and Φ=69° for both wings; $\bar{\phi}$=5.5° and 17.5° for the forewing and hindwing, respectively; geometrical angles of attack are approximately the same for fore- and hindwings. Morphological data for the insect have been given in Norberg (1972): the mass of the insect (m) is 754 mg; forewing length is 4.74 cm; hindwing length is 4.60 cm; the mean chord lengths of the forewing and the hindwing are 0.81 cm and 1.12 cm, respectively. In the present study, we assume that for the dragonfly, $\bar{\phi}$, n and Φ do not vary with flight speed [data in Azuma and Watanabe (1988) show that n hardly varies with flight speed and Φ is increased only at very high speed]. On the basis of the above data, we use the following parameters for the model dragonfly: the length of both wings (R) is 4.7 cm (S_f and S_h are 3.81 and 5.26 cm^2, respectively); the reference length (c) is 0.81 cm; $U=2\Phi nr_2$=2.5 m s^{-1}; $Re=Uc/\nu\approx1350$; $\tau_c=U/nc$=8.58. Norberg (1975) did not provide the rate of wing rotation during stroke reversal. Reavis and Luttges (1988) made measurements on some dragonflies and it was found that maximum $\dot{\alpha}$ was ~10 000–30 000 deg. s^{-1}. Here, $\dot{\alpha}$ is set as 20 000 deg. s^{-1}, giving $\Delta\tau_r$=3.36. In hovering, the body of dragonfly *Aeshna juncea* is horizontal (Norberg, 1975). We assume it is also horizontal at forward flight. The angle between the body axis and the stroke plane hardly changes (Azuma and Watanabe, 1988; Wakeling and Ellington, 1997b), therefore β at forward flight can be assumed to be the same as that at hovering [in Sun and Lan's (2004) study of hovering flight, β=52° was used; the same value is used here]. We also assume that at all speeds considered, geometrical angles of attack are the same for fore- and hindwings. In the present study, γ_d and J are varied systematically to study their effects, therefore they are known.

Now, the only kinematic parameters left to be specified are α_d and α_u. In the present study, α_d and α_u are not treated as known input parameters but are determined in the calculation process; they are chosen such that the computed mean vertical force of the wings approximately equals the insect weight and the computed mean thrust approximately equals the body drag. The mean vertical force coefficient required for balancing the weight ($C_{V,W}$) is defined as $C_{V,W}=mg/0.5\rho U^2(S_f+S_h)$; the body-drag coefficient ($C_{D,b}$) is defined as $C_{D,b}$=body-drag/$0.5\rho U^2(S_f+S_h)$. Using the above data, $C_{V,W}$ is computed as $C_{V,W}$=1.35. The body-drag of *Aeshna juncea* is not available. Here, the body-drag coefficients for dragonfly *Sympetrum sanguineum* (Wakeling and Ellington, 1997a) are used (converted to the current definition of $C_{D,b}$). Values of $C_{D,b}$ at various J are shown in Table 1.

Results

Force balance in the flight

In the present study, six advance ratios (J=0, 0.15, 0.30, 0.45, 0.60, 0.75; V_∞=0–3.1 m s^{-1}) and, at each J, four phase differences (γ_d=180°, 90°, 60° and 0°; hindwing leads the forewing motion), are considered. At a given set of J and γ_d, α_d and α_u are chosen such that the C_V approximately equals $C_{V,W}$, and C_T approximately equals $C_{D,b}$. The calculation procedure is as follows. At a given J and γ_d, a set of values of α_d and α_u is estimated (how the starting values are estimated is described below). The flow equations are solved and the corresponding C_V and C_T are calculated. C_V is compared with $C_{V,W}$ (1.35) and C_T is compared with $C_{D,b}$ (Table 1). If C_V is different from $C_{V,W}$, or C_T is different from $C_{D,b}$, α_d and α_u are adjusted. The calculations are repeated until the difference between C_V and $C_{V,W}$ is less than 0.05 and the difference between C_T and $C_{D,b}$ is less than ~0.01 (as will be seen below, in most cases, a difference between C_T and $C_{D,b}$ of less than 0.005 is achieved).

The case of J=0 (γ_d=180°) is computed first. For this case, values of α_d and α_u close to the real ones are available from

Table 1. *Body-drag coefficient*

J	0	0.15	0.30	0.45	0.60	0.75
V_∞ (m s^{-1})	0.0	0.62	1.23	1.85	2.47	3.08
Re_{body}	0.0	3115	6230	9346	12461	15576
$C_{D,b}$	0.0	0.004	0.020	0.045	0.080	0.125

J, advance ratio; V_∞, flight velocity; Re_{body}, body Reynolds number; $C_{D,b}$, body-drag coefficient.

Norberg (1975). For dragonfly *Aeshna juncea* hovering with γ_d=180°, Norberg (1975) observed that in the mid-portion of the downstroke, the wing chord was almost horizontal, and in the mid-portion of the upstroke it was close to the vertical; that is the real values of α_d and α_u should be around 50° and 20°, respectively (note that β=52°). α_d=50° and α_u=15° are used as the starting values, and the converged values of α_d and α_u are 52° and 8°, respectively. Using starting values that are not far from the real values can reduce the number of iterations. More importantly, there could be more than one solution due to the nonlinearity in aerodynamic force production, and by so doing, the calculation can generally converge to the realistic solution. Second, the case of J=0.15 (γ_d=180°) is computed, using the converged values of α_d and α_u of J=0 (γ_d=180°) as the starting values. Since J is not changed greatly, it is expected that these starting values are not very different from the realistic solution. The same is done, sequentially, for the cases of J=0.3, 0.45, 0.6 and 0.75 (γ_d=180°). Next, the case of J=0 (γ_d=90°) is computed, using the converged values of α_d and α_u at J=0 (γ_d=180°) as the starting values; then the cases of J=0.15–0.75 (γ_d=90°) are computed in the same way as in the corresponding cases of γ_d=180°. Finally, the cases of J=0–0.75, γ_d=60° and 0° are treated in a similar way.

The calculated results of α_d and α_u are shown in Table 2. Since, in each of the cases, the starting values of α_d and α_u are expected to be not far from the real values, it is reasonable to expect that these solutions are realistic. Let's examine how the calculated α_d and α_u vary with advance ratio, which can give some information on whether or not the solutions are realistic. As seen in Table 2, at a given γ_d, when J is increased, α_d decreases and α_u increases. This should be the correct trend of variation for the following reasons. When J is increased, in the downstroke the relative velocity of the wing increases and, to keep the total vertical force from increasing (vertical force is mainly produced during the downstroke and it needs to be equal to the weight of the dragonfly), α_d should decrease; in the upstroke, the relative velocity decreases and, to produce enough thrust (thrust is mainly produced during the upstroke and a larger thrust is needed as J is increased), α_u should increase. As also seen in Table 2, α_u increases with J at a relatively higher rate (α_u increases approximately from 8° to 65° when J changes from 0 to 0.75). This is reasonable because, if α_u does not increase with J fast enough, the effective angle of attack of the wing would become negative (generally, operating at negative effective angle of attack is not realistic). The variations of α_d

Table 2. *Mean force coefficient and angles of attack at balance flight*

γ_d	J	α_d (deg.)	α_u (deg.)	$\overline{C}_{V,f}$	$\overline{C}_{V,h}$	$\overline{C}_{T,f}$	$\overline{C}_{T,h}$	$\overline{C}_V$	$\overline{C}_T$
180°	0	52.0	8.0	0.56	0.79	0.022	–0.037	1.35	–0.015
	0.15	44.0	14.0	0.68	0.70	0.063	–0.059	1.38	0.004
	0.30	36.0	22.0	0.66	0.69	0.066	–0.049	1.35	0.017
	0.45	33.0	36.0	0.64	0.73	0.074	–0.024	1.37	0.050
	0.60	32.0	51.0	0.60	0.72	0.077	0.008	1.32	0.085
	0.75	34.0	65.0	0.62	0.75	0.083	0.066	1.37	0.149
90°	0	52.0	7.0	0.54	0.78	0.023	–0.020	1.32	0.003
	0.15	42.0	13.2	0.62	0.74	0.076	–0.074	1.36	0.002
	0.30	33.0	21.4	0.57	0.74	0.064	–0.048	1.31	0.016
	0.45	31.0	35.3	0.57	0.77	0.049	–0.004	1.34	0.045
	0.60	31.0	50.0	0.57	0.74	0.041	0.044	1.32	0.085
	0.75	33.0	64.0	0.58	0.75	0.055	0.096	1.33	0.152
60°	0	48.0	5.5	0.56	0.76	0.050	–0.054	1.32	–0.004
	0.15	40.0	12.5	0.63	0.76	0.089	–0.084	1.39	0.005
	0.30	32.0	21.8	0.57	0.75	0.076	–0.058	1.32	0.018
	0.45	31.0	35.0	0.59	0.79	0.053	–0.010	1.38	0.043
	0.60	31.0	50.0	0.59	0.74	0.049	0.040	1.33	0.089
	0.75	33.0	64.0	0.61	0.71	0.060	0.108	1.32	0.168
0°	0	45.0	6.8	0.60	0.75	0.138	–0.134	1.35	0.004
	0.15	38.0	9.7	0.65	0.71	0.124	–0.120	1.36	0.004
	0.30	31.5	19.9	0.61	0.72	0.103	–0.085	1.33	0.018
	0.45	31.5	35.0	0.63	0.71	0.091	–0.028	1.34	0.063
	0.60	31.5	48.5	0.62	0.67	0.064	0.002	1.29	0.066
	0.75	35.0	63.0	0.72	0.66	0.072	0.086	1.38	0.158

γ_d, phase difference angle between fore- and hindwings; J, advance ratio; α_d and α_u, middle stroke angle of attack in the down- and upstrokes, respectively; $\overline{C}_V$ and $\overline{C}_T$, mean total vertical and horizontal force coefficients, respectively; $\overline{C}_{V,f}$ and $\overline{C}_{T,f}$, mean vertical and horizontal force coefficients of the forewing, respectively; $\overline{C}_{V,h}$ and $\overline{C}_{T,h}$, mean vertical and horizontal force coefficients of the hindwing, respectively.

and α_u with J also show that it is reasonable to expect that the solutions are realistic.

In Table 2, the mean total force coefficients ($\overline{C}_V$, $\overline{C}_T$), and the mean force coefficients of the forewing ($\overline{C}_{V,f}$, $\overline{C}_{T,f}$) and hindwing ($\overline{C}_{V,h}$, $\overline{C}_{T,h}$) are also given ($\overline{C}_{V,f}$, $\overline{C}_{T,f}$, etc. could show how much aerodynamic force is produced by the forewing or by the hindwing). $\overline{C}_V$ is close to $C_{V,W}$ and $\overline{C}_T$ is closed to $C_{D,b}$, as they should be. The mean thrust (the body-drag) is much smaller than the mean vertical force (the weight); e.g. at J=0, 0.3 and 0.6, $\overline{C}_T$ is only 0, 1.4 and 6.6% of $\overline{C}_V$, respectively. At a given J, α_d and α_u do not change greatly when γ_d is varied. For example, at J=0.15, α_d and α_u are 44° and 14°, respectively, at γ_d=180°; 42° and 13.2° at γ_d=90°; 40° and 12.5° at γ_d=60°; 38° and 9.7° at γ_d=0°.

The fact that changing γ_d from 180° to 0° does not influence α_d and α_u values greatly indicates that the forewing–hindwing interaction might not be very strong. This is because the interaction between the wings is expected to be sensitive to the relative motion, or to the phase difference, between the wings, and if strong interaction exits, the values of α_d and α_u would be greatly influenced by varying γ_d from 180° to 0°.

The time courses of the aerodynamic forces

The effects of phasing

Fig. 3 gives the time courses of C_V and C_T in one cycle for various forewing–hindwing phase differences for hovering flight (J=0). For a clear description of the time courses of the forces and flows, we express time during a cycle as a non-dimensional parameter, $\hat{t}$, such that $\hat{t}$=0 at the start of the downstroke of the hindwing and $\hat{t}$=1 at the end of the following upstroke. At γ_d=180°, there are two large C_V peaks in one cycle, one in the first half-cycle ($\hat{t}$=0–0.5) and the other in the second half-cycle ($\hat{t}$=0.5–1.0) [this case has been investigated in Sun and Lan (2004) and is included here for comparison]. When the phase difference is changed to γ_d=90°, these two peaks merge into a large C_V peak between $\hat{t}$=0 and $\hat{t}$=0.75. The result at γ_d=60° is similar to that at γ_d=90°, except that the C_V peak is between $\hat{t}$=0 and $\hat{t}$=0.62 and is higher. For the case of γ_d=0°, the C_V peak is between $\hat{t}$=0 and $\hat{t}$=0.5 and is even higher. C_V is the sum of $C_{V,f}$ and $C_{V,h}$. Fig. 4 gives the time courses of $C_{V,f}$ and $C_{V,h}$ for the above cases. In all these cases, the hindwing produces a large $C_{V,h}$ peak during its downstroke and a very small $C_{V,h}$ during its upstroke; this is also true for the forewing. At γ_d=180°, the downstroke of the hindwing is in the first half-cycle ($\hat{t}$=0–0.5) and the downstroke of the forewing is in the second half-cycle ($\hat{t}$=0.5–1.0), resulting in the two C_V peaks (one between $\hat{t}$=0 and $\hat{t}$=0.5 and the other between $\hat{t}$=0.5 and $\hat{t}$=1.0; see the C_V curve for γ_d=180° in Fig. 3). At γ_d=90°, the downstroke of the hindwing is still in the first half-cycle (between $\hat{t}$=0 and $\hat{t}$=0.5), but the downstroke of the forewing is between $\hat{t}$=0.25 and $\hat{t}$=0.75, resulting in the C_V peak between $\hat{t}$=0 and $\hat{t}$=0.75 (see the C_V curve for γ_d=90° in Fig. 3). The C_V peak for the cases of γ_d=60° and 0° in Fig. 3 can be explained similarly.

Fig. 5 gives the C_V and C_T results for forward flight at J=0.3. The effects of varying the phasing are similar to those in the cases of J=0, i.e. when γ_d is decreased from 180° to 90° (and below), the two C_V peaks (between $\hat{t}$=0 and $\hat{t}$=0.5 and between $\hat{t}$=0.5 and $\hat{t}$=1.0, respectively) merge into one C_V peak. This is generally true for other advance ratios considered.

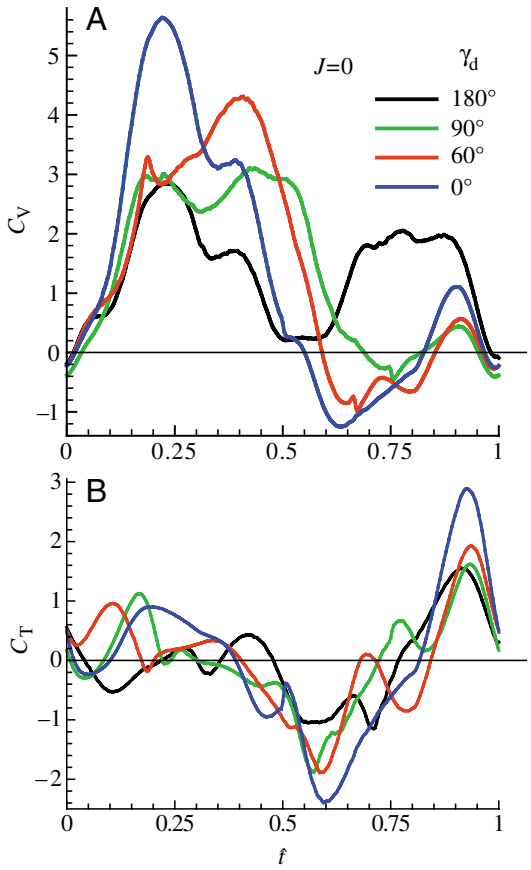

Fig. 3. Time courses of (A) total vertical force coefficient (C_V) and (B) total thrust coefficient (C_T) in one cycle at various γ_d (hovering, J=0). γ_d, difference in phase angle between the hindwing and forewing; J, advance ratio; $\hat{t}$, non-dimensional time.

The effects of flight speed

Fig. 6 gives the time courses of C_V and C_T in one cycle for various advance ratios. For clarity, only the C_V and C_T curves for J=0, 0.3 and 0.6 are plotted [the C_V (or C_T) curve for J=0.15 is between those of J=0 and 0.3; the C_V (or C_T) curve for J=0.45 is between those of J=0.3 and 0.6; and the C_V (or C_T) curve for J=0.75 is close to that for J=0.6].

At γ_d=180° (Fig. 6A), as J is increased, the distributions of C_V in the first half-cycle ($\hat{t}$=0–0.5) change greatly: C_V between $\hat{t}$=0 and $\hat{t}$=0.3 is decreased and C_V around $\hat{t}$=0.4 is increased. As discussed above, C_V in the first half-cycle is due to the hindwing downstroke. The decrease in C_V between $\hat{t}$=0 and $\hat{t}$=0.3 is caused mainly by two factors; (1) α_d of the hindwing is smaller at higher speeds (Table 2) and (2) at higher speeds, the forewing–hindwing interaction decreases the vertical force on the hindwing in this period (see below). The large increase in C_V around $\hat{t}$=0.4 is due to the effect of pitching-up rotation of the hindwing. It is known that when a wing pitches up in an

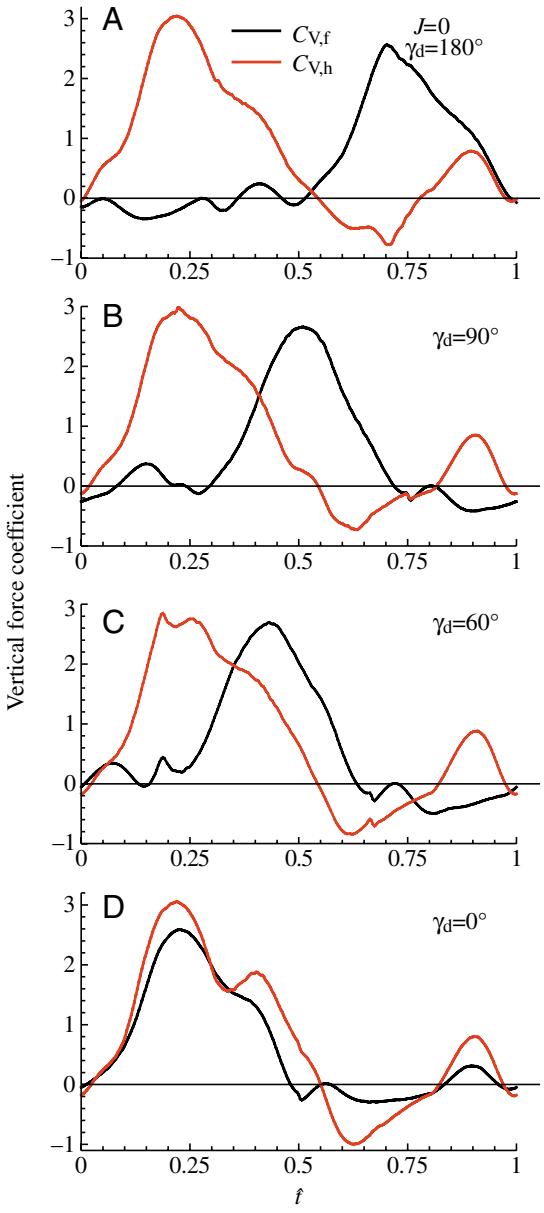

Fig. 4. Time courses of vertical force coefficients of forewing ($C_{V,f}$) and hindwing ($C_{V,h}$) at hovering (J=0). (A) γ_d=180°, (B) γ_d=90°, (C) γ_d=60°, (D) γ_d=0°. γ_d, difference in phase angle between the hindwing and forewing; J, advance ratio; $\hat{t}$, non-dimensional time.

incoming flow, large aerodynamic forces could be produced; the higher the incoming flow speed, the larger the forces (Dickinson et al., 1999; Lan and Sun, 2001; Sun and Tang, 2002). The hindwing undergoes pitching-up rotation at $\hat{t}$=0.4. At higher J, the relative velocity is larger and, in addition, the portion of wing area behind the rotation-axis is relatively large for the hindwing (see Fig. 1A), resulting in the large C_V around $\hat{t}$=0.4.

At γ_d=90°, 60° and 0° (Fig. 6C, E and G, respectively), the effects of increasing J on C_V are similar to those in the case of γ_d=180°.

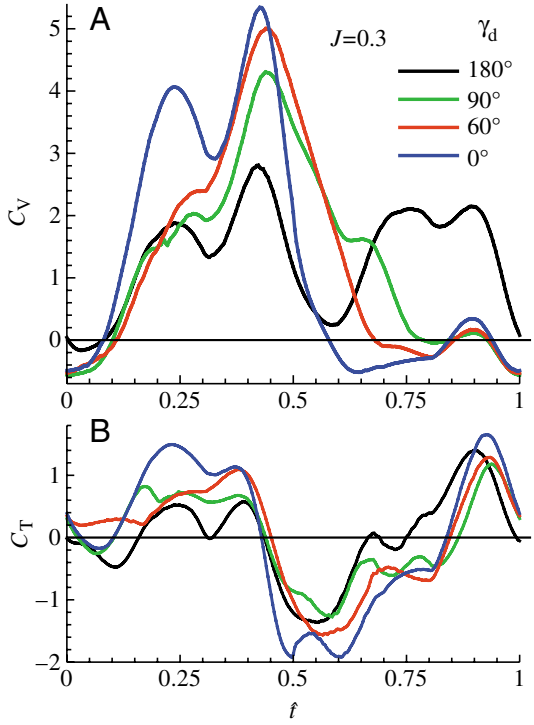

Fig. 5. Time courses of (A) total vertical force coefficient (C_V) and (B) total thrust coefficient (C_T) in one cycle at various γ_d (forward flight, J=0.3). γ_d, difference in phase angle between the hindwing and forewing; J, advance ratio; $\hat{t}$, non-dimensional time.

The lift and drag coefficients of the fore- and hindwings

The vertical force coefficient of a wing is related to the lift and drag coefficients (see Eqn 1). Fig. 7 shows the vertical force, lift and drag coefficients of the hindwing and the forewing, respectively, for the case of J=0.3 and γ_d=180°. Fig. 8 shows the corresponding results for the case of J=0.6 and γ_d=180°. It is seen that for the forewing or the hindwing, the drag coefficient is larger than, or close to, the lift coefficient. Furthermore, β is large (52°). As a result (see Eqn 1), a large part of the vertical force coefficient is contributed by the drag coefficient. This is also true for other flight conditions. Our computations show that for all cases considered in the present study, 55–67% of the total vertical force is contributed by the drag of the wings. The results here are for hovering and forward flight conditions. For hovering, similar results have been obtained previously: Sun and Lan (2004) showed that for the same dragonfly as in the present study, 65% of the weight-supporting force is contributed by the wing drag; Wang (2004), using two-dimensional model, showed that a dragonfly might use drag to support about three-quarters of its weight.

The flows around the forewing and the hindwing

Here, we present flows around the forewing and the hindwing for six representative cases: γ_d=180° and J=0, 0.3 and 0.6; γ_d=60° and J=0, 0.3 and 0.6. Figs 9–11 show the

contours of the non-dimensional spanwise component of vorticity at half-wing length at various times of the stroke cycle, for the cases J=0, 0.3 and 0.6 of γ_d=180°; Figs 12–14 show the corresponding results for the cases of γ_d=60°. Since the variation in J causes considerable changes in α_d and α_u, to guard against possible misinterpretation of the results, in each

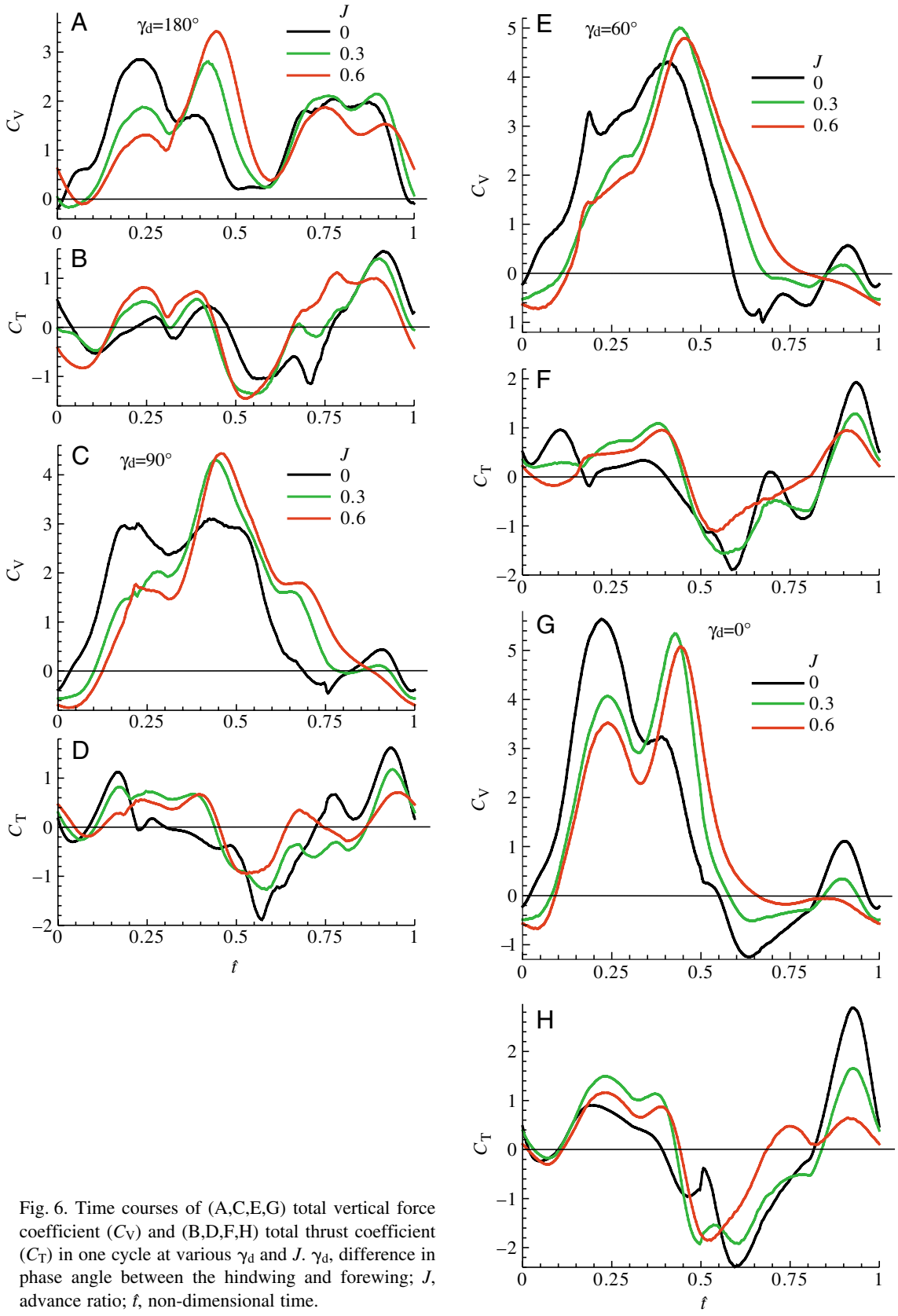

Fig. 6. Time courses of (A,C,E,G) total vertical force coefficient (C_V) and (B,D,F,H) total thrust coefficient (C_T) in one cycle at various γ_d and J. γ_d, difference in phase angle between the hindwing and forewing; J, advance ratio; $\hat{t}$, non-dimensional time.

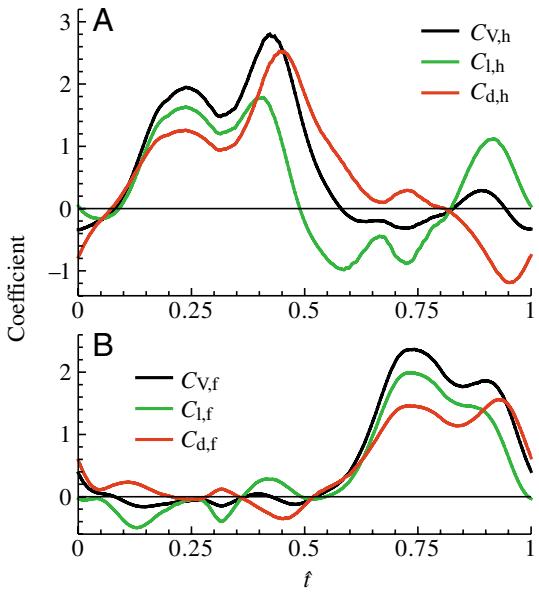

Fig. 7. Time courses of vertical force, lift and drag coefficients for the hindwing (A) and the forewing (B) in one cycle at γ_d=180° and J=0.3. $C_{V,h}$, $C_{l,h}$ and $C_{d,h}$, vertical force, lift and drag coefficients of the hindwing, respectively; $C_{V,f}$, $C_{l,f}$ and $C_{d,f}$, vertical force, lift and drag coefficients of the forewing, respectively; γ_d, difference in phase angle between the hindwing and forewing; J, advance ratio; $\hat{t}$, non-dimensional time.

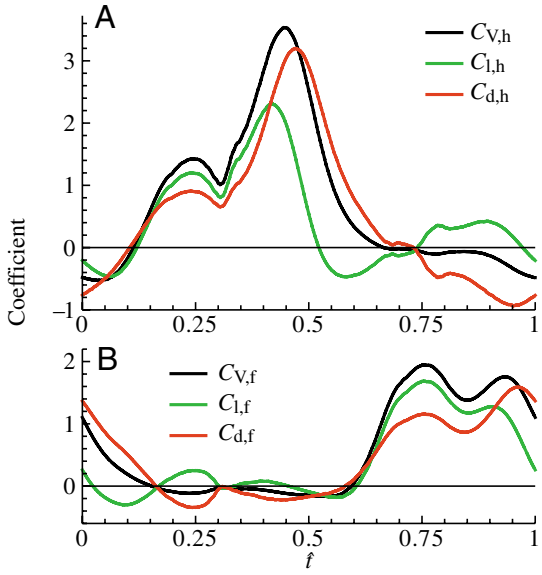

Fig. 8. Time courses of vertical force, lift and drag coefficients for the hindwing (A) and the forewing (B) in one cycle at γ_d=180° and J=0.6. $C_{V,h}$, $C_{l,h}$ and $C_{d,h}$, vertical force, lift and drag coefficients of the hindwing, respectively; $C_{V,f}$, $C_{l,f}$ and $C_{d,f}$, vertical force, lift and drag coefficients of the forewing, respectively; γ_d, difference in phase angle between the hindwing and forewing; J, advance ratio; $\hat{t}$, non-dimensional time.

of Figs 9–14, α_d and α_u are specified at the same time as J (this is also done in Fig. 15). In Figs 9–14, τ_1, τ_2 and τ_3 represent the times at $0.1\tau_c$ after the start of the downstroke, the mid-downstroke and $0.4\tau_c$ after the start of the downstroke of a wing, respectively; τ_4, τ_5 and τ_6 represent the corresponding times of the upstroke of the wing.

First, we examine the cases of γ_d=180°. At J=0 for the forewing (Fig. 9A), during the downstroke a LEV of large size appears (see plots at τ_2 and τ_3 in Fig. 9A); during the upstroke, there is no LEV and the vorticity layers on the upper and lower surfaces of the wing are approximately the same (see plots at τ_5 and τ_6 in Fig. 9A), indicating that the effective angle of attack is close to zero. For the hindwing (Fig. 9B), during the downstroke the flows are generally similar to those of the forewing, except that the LEV is a little smaller and a vortex layer shed from the trailing edge (trailing-edge vortex layer) of the forewing is around the hindwing at its mid-upstroke (see plot at τ_5 in Fig. 9B). At J=0.3 (Fig. 10), the LEVs of the wings during their downstrokes are smaller than those at J=0 (compare Fig. 10 with Fig. 9); in fact, the LEV of the hindwing has the form of a thick vortex layer (see plots at τ_2 and τ_3 in Fig. 10B), indicating that the flow is effectively attached. Another difference is that the trailing-edge vortex layer of the forewing is less close to the hindwing at its mid-upstroke than in the case of J=0 (comparing the plot at τ_5 in Fig. 10B with the plot at τ_5 in Fig. 9B). At J=0.6 (Fig. 11), the LEVs of both the forewing and hindwing during their downstrokes have the form of a thick vortex layer (see plots at τ_2 and τ_3 in Fig. 11A and Fig. 11B), indicating that flows are effectively attached. The flow attachment during the downstrokes at relatively large J can be clearly seen from the sectional streamline plots shown in Fig. 15: as J increases, flows around the forewing and hindwing become more and more attached.

Next, we examine the cases of γ_d=60° (Figs 12–14). The flows vary with J in the same way as in the cases of γ_d=180° discussed above; that is, as J increases, the LEVs on the forewing and the hindwing downstrokes decease in size (becoming a vortex layer at relatively large J), and the hindwing in its downstroke meets less and less of the trailing-edge vortex layer of the forewing (compare Figs 12, 13 and 14). At a given J, the flows of the fore- and hindwings are not greatly different from those in the case of γ_d=180°, except that the hindwing in its upstroke meets the trailing-edge vortex layer of the forewing at an earlier time (compare Figs 12, 13 and 14 with Figs 9, 10 and 11, respectively). The fact that there do not exist large differences between the flows for γ_d=60° and γ_d=180° indicates that the forewing–hindwing interaction might not be very strong.

The forewing–hindwing interaction

In order to obtain quantitative data on the interaction between the fore- and hindwings, we made two more sets of computations. In the first set, the hindwing was taken away and the flows around the single forewing were computed; in the second set, the forewing was taken away and the flows around the single hindwing were computed. The vertical force and thrust for the single forewing are denoted as V_{sf} and T_{sf}, respectively; those for the single hindwing are denoted as V_{sh}

and T_{sh}. The coefficients of V_{sf}, T_{sf}, V_{sh} and T_{sh} are denoted as $C_{V,sf}$, $C_{T,sf}$, $C_{V,sh}$ and $C_{T,sh}$, respectively, and are defined as:

$$C_{V,sf} = V_{sf} / [0.5\rho U^2 (S_f + S_h)], \text{ etc.} \quad (8)$$

Note that they are defined in the same way as in the case of two wings in interaction (see Eqn 3).

Figs 16–19 compare the time courses of $C_{V,sf}$, $C_{V,sh}$, $C_{T,sf}$ and $C_{T,sh}$ with those of $C_{V,f}$, $C_{V,h}$, $C_{T,f}$ and $C_{T,h}$, respectively. The differences between $C_{V,sf}$ and $C_{V,f}$, etc., show the interaction effects. At a given γ_d and J (e.g. γ_d=180° and J=0.6; Fig. 16E), the vertical force coefficient of a wing is decreased at certain periods and increased at some other periods of a cycle due to forewing–hindwing interaction. When J is varied (e.g. comparing Fig. 16A,C,E) or γ_d is varied (e.g. comparing Figs 16A, 17A and 18A), the interaction effect occurs at different periods of the cycle and its strength may change. This is because, at a given time in the stroke cycle, a wing is at a different position relative to the wake of the other wing when J or γ_d is varied.

The total vertical force without interaction (V_{NI}) is the sum

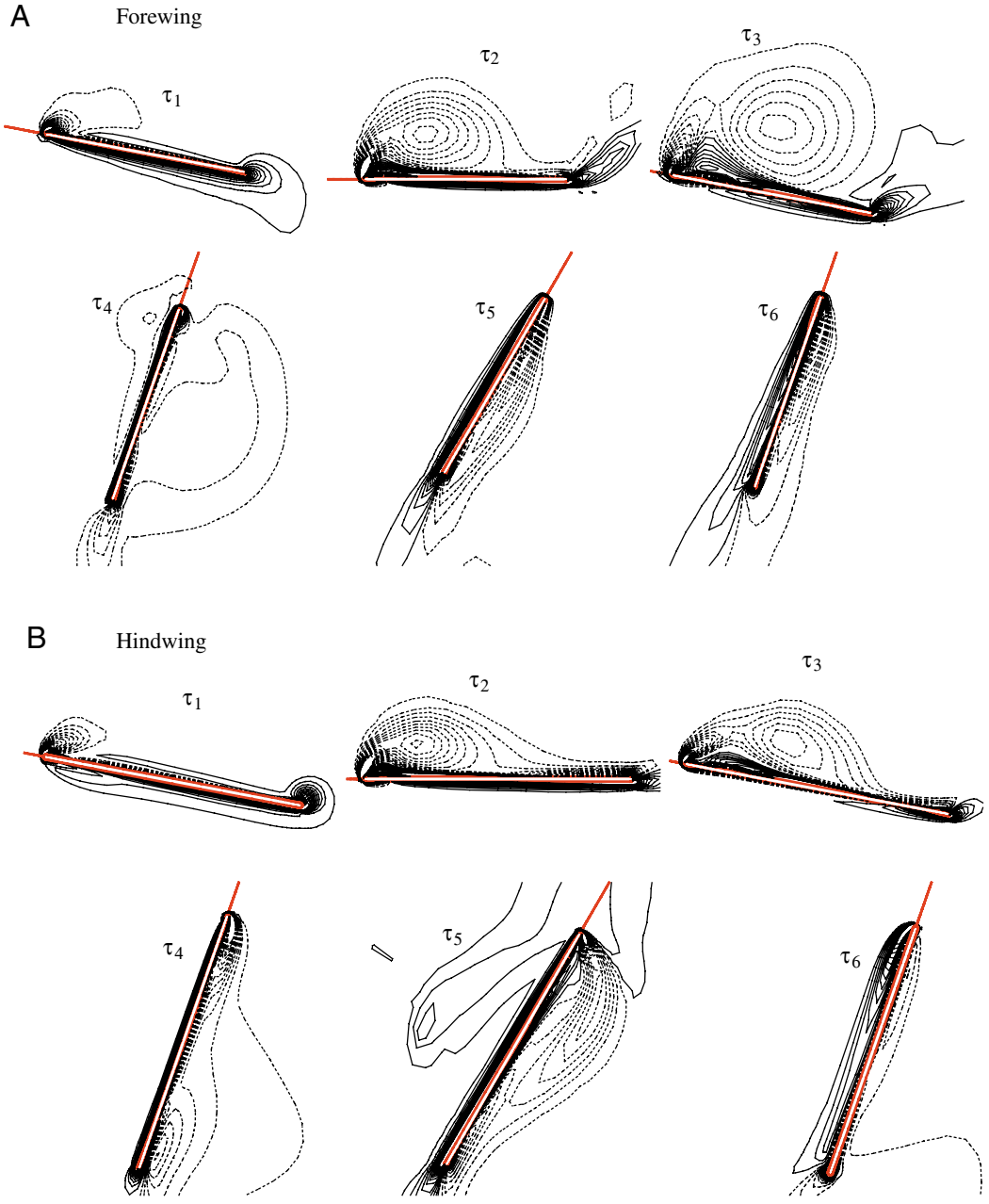

Fig. 9. Plot of spanwise component of vorticity at half-wing length at various times in a stroke cycle for the forewing (A) and the hindwing (B) at γ_d=180°, J=0 (α_d=52° and α_u=8°). Solid and broken lines indicate positive and negative vorticity, respectively; the magnitude of non-dimensional vorticity at the outer contour is 1 and the contour internal is 3. γ_d, difference in phase angle between the hindwing and forewing; J, advance ratio; α_d and α_u, geometric angles of attack in the down- and upstrokes, respectively; τ, non-dimensional time.

of V_{sf} and V_{sh}. The coefficient of V_{NI} is denoted as $C_{V,NI}$ and defined as:

$$C_{V,NI} = V_{NI} / [0.5\rho U^2 (S_f + S_h)], = C_{V,sf} + C_{V,sh} . \quad (9)$$

Let $\overline{C}_{V,NI}$ be the mean value of $C_{V,NI}$. Thus $\Delta\hat{C}_V=(\overline{C}_V-\overline{C}_{V,NI})/\overline{C}_{V,NI}$ represents the percentage of increment in mean total vertical force coefficient due to the forewing–hindwing interaction (when $\Delta\hat{C}_V$ is negative, the interaction is detrimental to vertical force generation). The value of $\Delta\hat{C}_V$ is given in Table 3. From the total vertical force and the total thrust, the total resultant force can be calculated. The increment in mean total resultant force coefficient due to the forewing–hindwing interaction is obtained in the same way as above, which is also given in Table 3. It is very close to $\Delta\hat{C}_V$. This is because, under the present flight conditions, the wings produce a much larger vertical force than thrust. As seen in Table 3, at all phase angles and advance ratios considered, the interaction is detrimental to the vertical force (or resultant force) generation. At hovering, the interaction reduces the mean total vertical force coefficient (or the mean total resultant

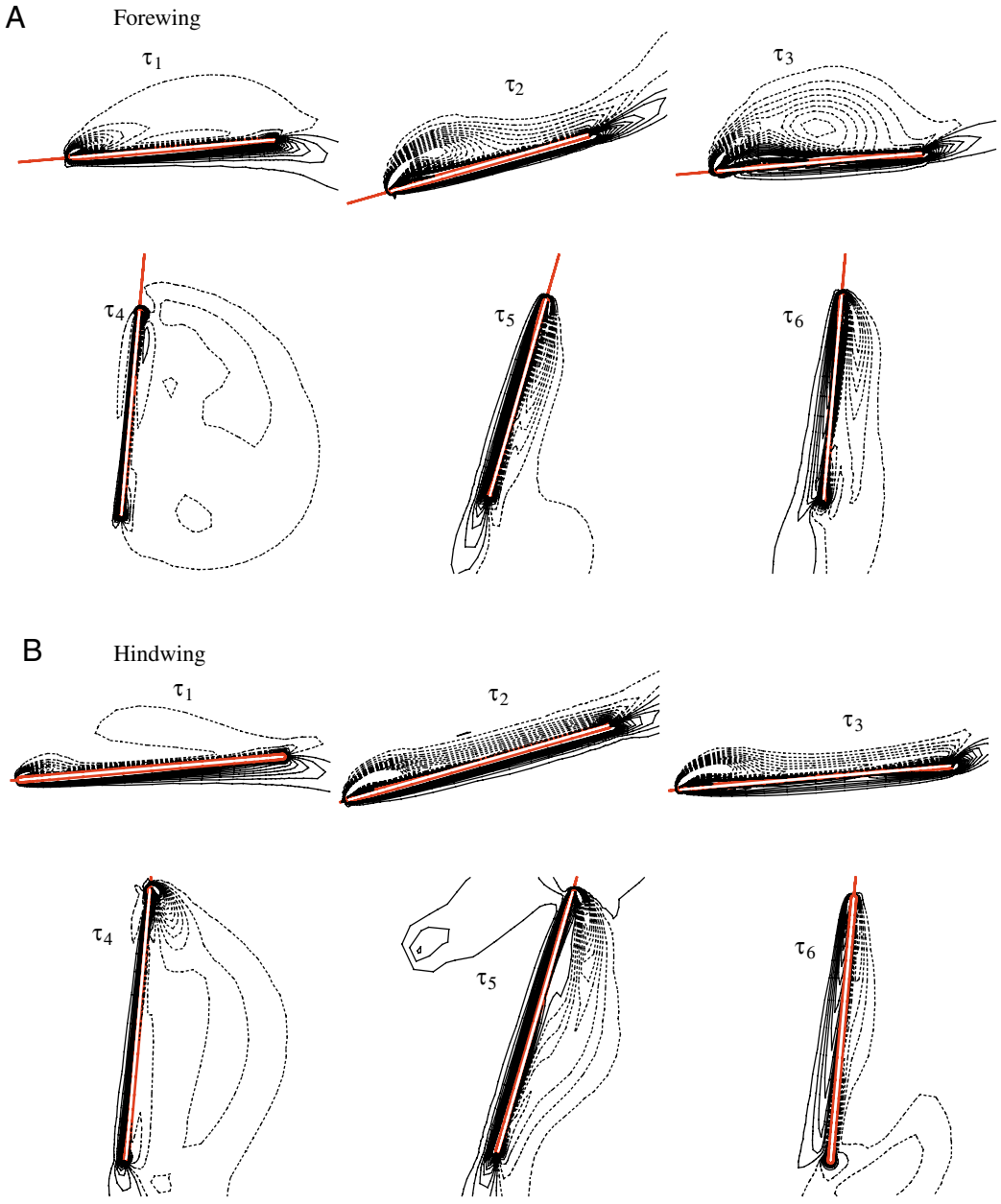

Fig. 10. Plot of spanwise component of vorticity at half-wing length at various time in a stroke cycle for the forewing (A) and the hindwing (B), at γ_d=180°, J=0.3 (α_d=36° and α_u=22°). Solid and broken lines indicate positive and negative vorticity, respectively; the magnitude of non-dimensional vorticity at the outer contour is 1 and the contour internal is 3. γ_d, difference in phase angle between the hindwing and forewing; J, advance ratio; α_d and α_u, geometric angles of attack in the down- and upstrokes, respectively; τ, non-dimensional time.

force coefficient) by around 15% for γ_d=180° and 90°, 8% for γ_d=60°, and 3% for γ_d=0°. As J increases, for γ_d=180°, 90° and 60°, the reduction decreases; but for γ_d=0°, the reduction changes little from hovering to medium advance ratios (J=0–0.3) and increases to 6–13% at higher advance ratios (J=0.45–0.75).

Recently, Maybury and Lehmann (2004) conducted experiments on interaction between two robotic wings. In their experiment, the two wings are stacked vertically (forewing on the top), the stroke planes are horizontal and the wings operate in still air. Although their experimental set-up is different from the set-up of our simulation, there is some resemblance between their experiment and our hovering simulation: the hindwing operates in the wake of the forewing and the forewing is also influenced by the disturbed flow due to the hindwing. Thus, the results on interaction effects obtained by these two studies might be similar to some extent. Data in fig. 3D of Maybury and Lehmann (2004) show that between a phase shift of 0 and 50% of the stroke cycle (γ_d≈0–180°), the total vertical force is reduced by approximately 6–16% due to the interaction. The results in the present study show that between γ_d≈60–180°, the total

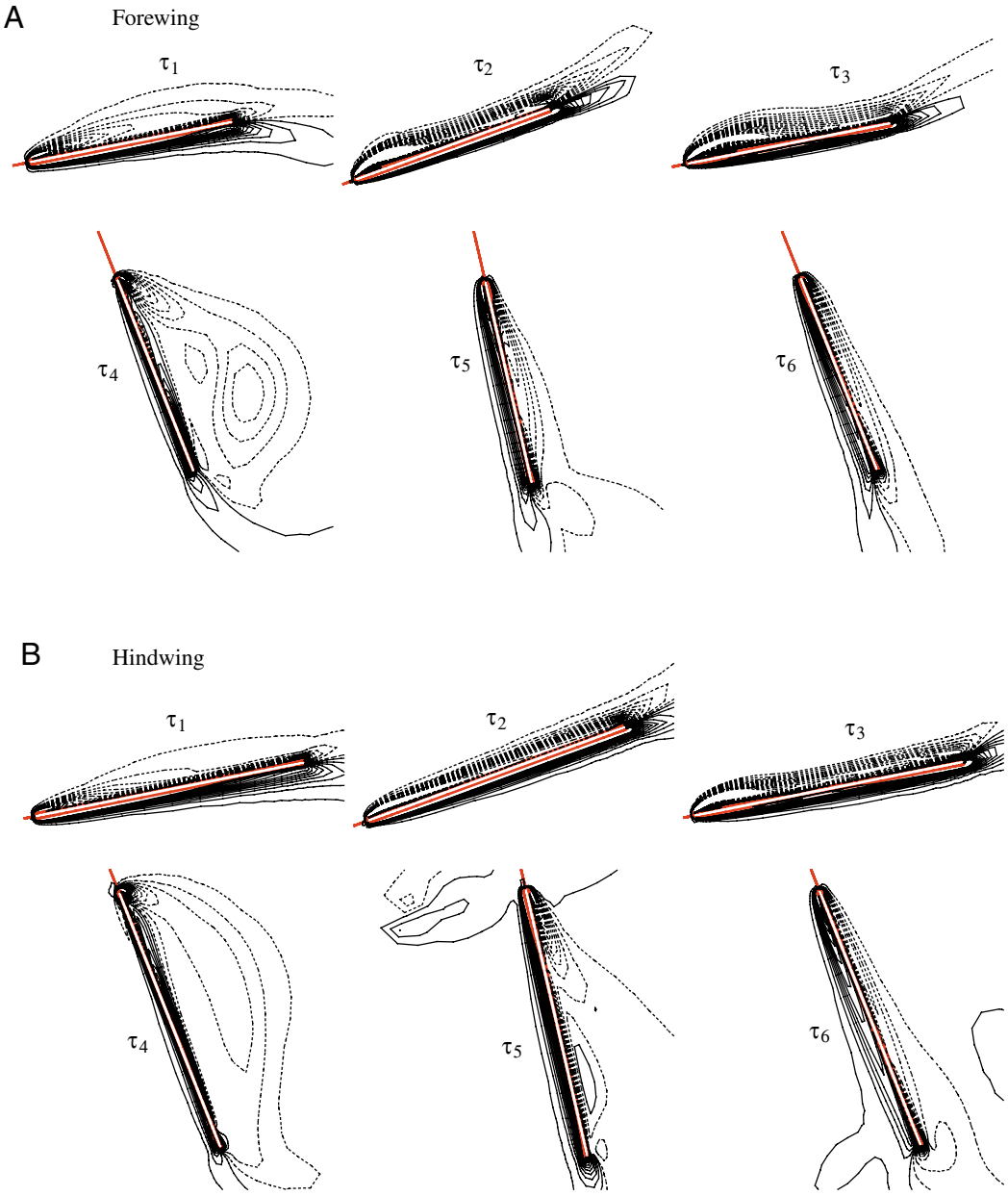

Fig. 11. Plot of spanwise component of vorticity at half-wing length at various time in a stroke cycle for the forewing (A) and the hindwing (B), at γ_d=180°, J=0.6 (α_d=32° and α_u=51°). Solid and broken lines indicate positive and negative vorticity, respectively; the magnitude of non-dimensional vorticity at the outer contour is 1 and the contour internal is 3. γ_d, difference in phase angle between the hindwing and forewing; J, advance ratio; α_d and α_u, geometric angles of attack in the down- and upstrokes, respectively; τ, non-dimensional time.

vertical force is reduced by 7.8–15% due to the interaction (see Table 3, J=0).

Discussion

The forewing–hindwing interaction is detrimental to the vertical force generation

Results in the present computations (24 cases of different phasing and advance ratios) show that for the forewing or the hindwing, although its vertical force coefficient at certain periods of the stroke cycle can be slightly increased by the forewing–hindwing interaction effects, its mean vertical force coefficient is decreased by the interaction effects. That is, the forewing–hindwing interaction is detrimental to the vertical force generation (and also to the resultant force generation; as mentioned above, vertical force is very close to the resultant force because the thrust is much smaller than the vertical force). This is remarkable but not totally unexpected. For all the cases considered, each of the fore- and hindwings produces a mean vertical force coefficient close to half that needed to support the insect weight (see $\bar{C}_{V,f}$ and $\bar{C}_{V,h}$ in Table 2). In producing an upward force, a downward flow must be

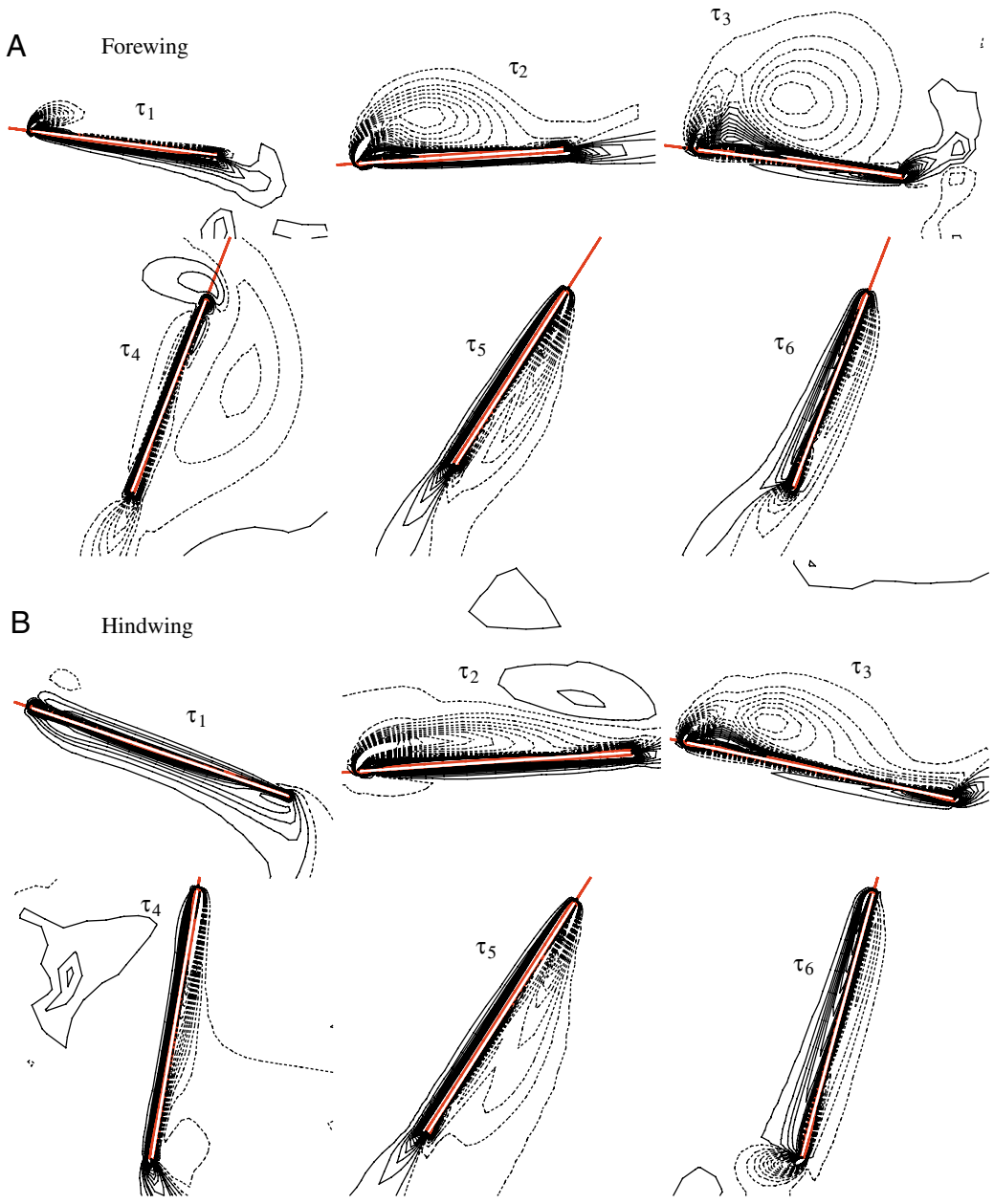

Fig. 12. Plot of spanwise component of vorticity at half-wing length at various time in a stroke cycle for the forewing (A) and the hindwing (B), at γ_d=60°, J=0.0 (α_d=48° and α_u=5.5°). Solid and broken lines indicate positive and negative vorticity, respectively; the magnitude of non-dimensional vorticity at the outer contour is 1 and the contour internal is 3. γ_d, difference in phase angle between the hindwing and forewing; J, advance ratio; α_d and α_u, geometric angles of attack in the down- and upstrokes, respectively; τ, non-dimensional time.

generated. Thus, in general, a wing would move in the downwash-velocity field induced by the other wing, reducing its vertical force.

Somps and Luttges (1985), based on their experiments, suggested that forewing–hindwing interaction might enhance aerodynamic force production. Results in the present study, however, show that the interaction is detrimental. It is of interest to discuss the present results in relation to those of Somps and Luttges (1985). In their experiment with a tethered dragonfly (in still air; wings flapping with $\gamma_d \approx 80°$), Somps and Luttges (1985) measured the time course of the total vertical force, which has a single large peak in each cycle (see fig. 2c of Somps and Luttges, 1985); the mean vertical force is more than twice the body weight. Based on the fact that one single large vertical force peak is produced in each cycle (rather than the double peaks they expected from the sum of the forces produced independently by the fore- and hindwings), they considered that the forewing–hindwing interaction must be strong and suggested that it played an important role in generating the large vertical force. Our vertical force time histories for $\gamma_d=60°$ and 90° at hovering are very similar to those in Somps and Luttges (1985), also having a single large

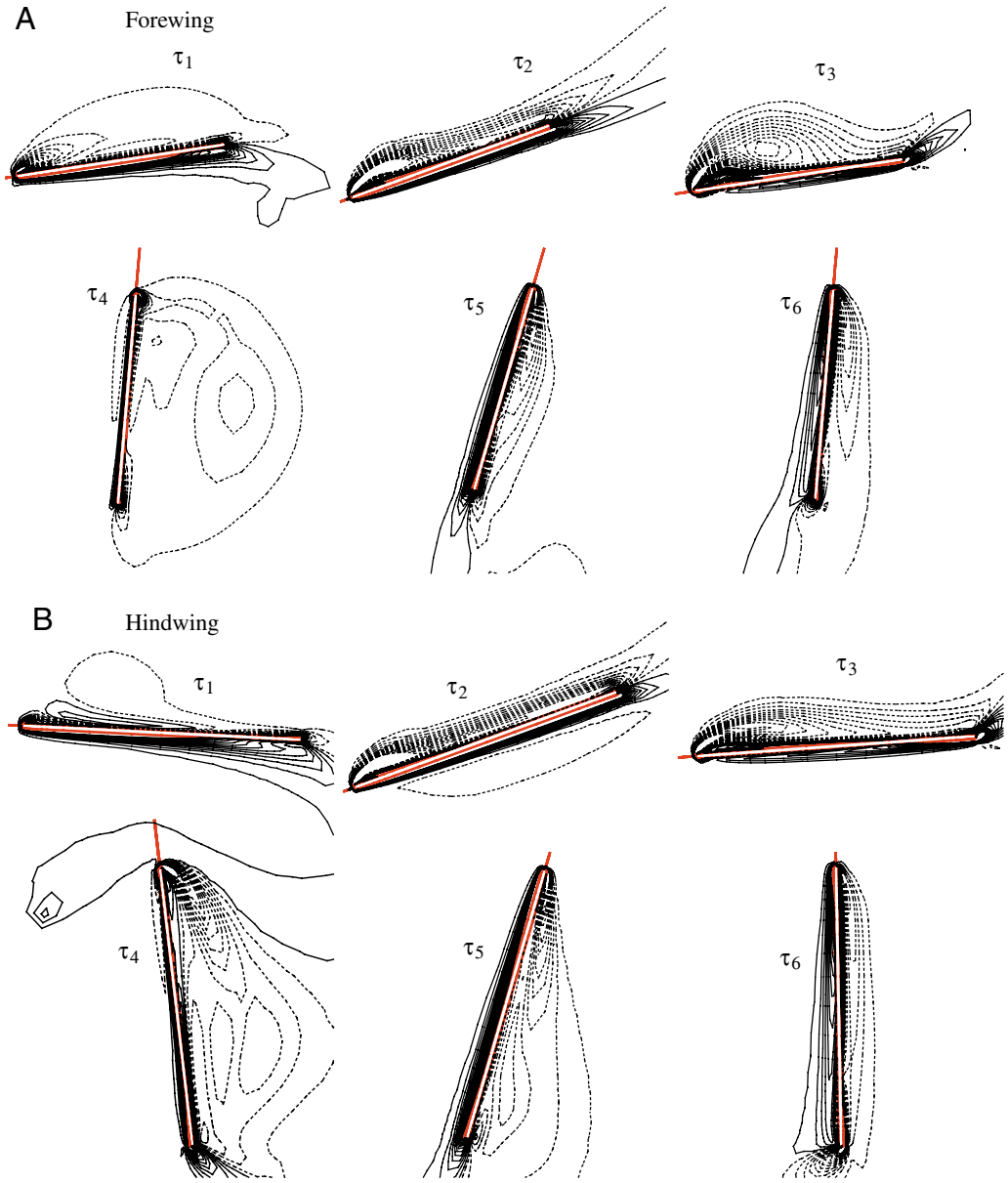

Fig. 13. Plot of spanwise component of vorticity at half-wing length at various time in a stroke cycle for the forewing (A) and the hindwing (B), at $\gamma_d=60°$, $J=0.3$ ($\alpha_d=32°$ and $\alpha_u=21.8°$). Solid and broken lines indicate positive and negative vorticity, respectively; the magnitude of non-dimensional vorticity at the outer contour is 1 and the contour internal is 3. γ_d, difference in phase angle between the hindwing and forewing; J, advance ratio; α_d and α_u, geometric angles of attack in the down- and upstrokes, respectively; τ, non-dimensional time.

peak in each cycle [compare the C_V curve for γ_d=60° or 90° in Fig. 3A with the curve in fig. 2c of Somps and Luttges (1985)]. However, analyses in the present study clearly show that the large single force peak is not due to forewing–hindwing interaction but rather to the overlap of the single force peak produced by the hindwing with that by the forewing.

Separated and attached flows

As seen in Figs 9–15, at hovering (J=0), flows on both the forewing and hindwing during the loaded downstroke are separated and large LEVs exist. As J increases, the LEVs become smaller and smaller and the flows become more and more attached. The flows of the hindwing downstroke are effectively attached at J=0.3 and those of the forewing downstroke are effectively attached at J=0.6 (see e.g. Fig. 15). That is, in producing the aerodynamic forces needed for flight, the model dragonfly uses separated flows with LEVs at hovering and low J, uses both separated and attached flows at medium J, and uses attached flow at high J.

At hovering and low J, the relative velocity of a wing is mainly due to the flapping motion and is relatively low. Thus, high 'aerodynamic force coefficients' are needed (in the present section, aerodynamic force coefficients are coefficients

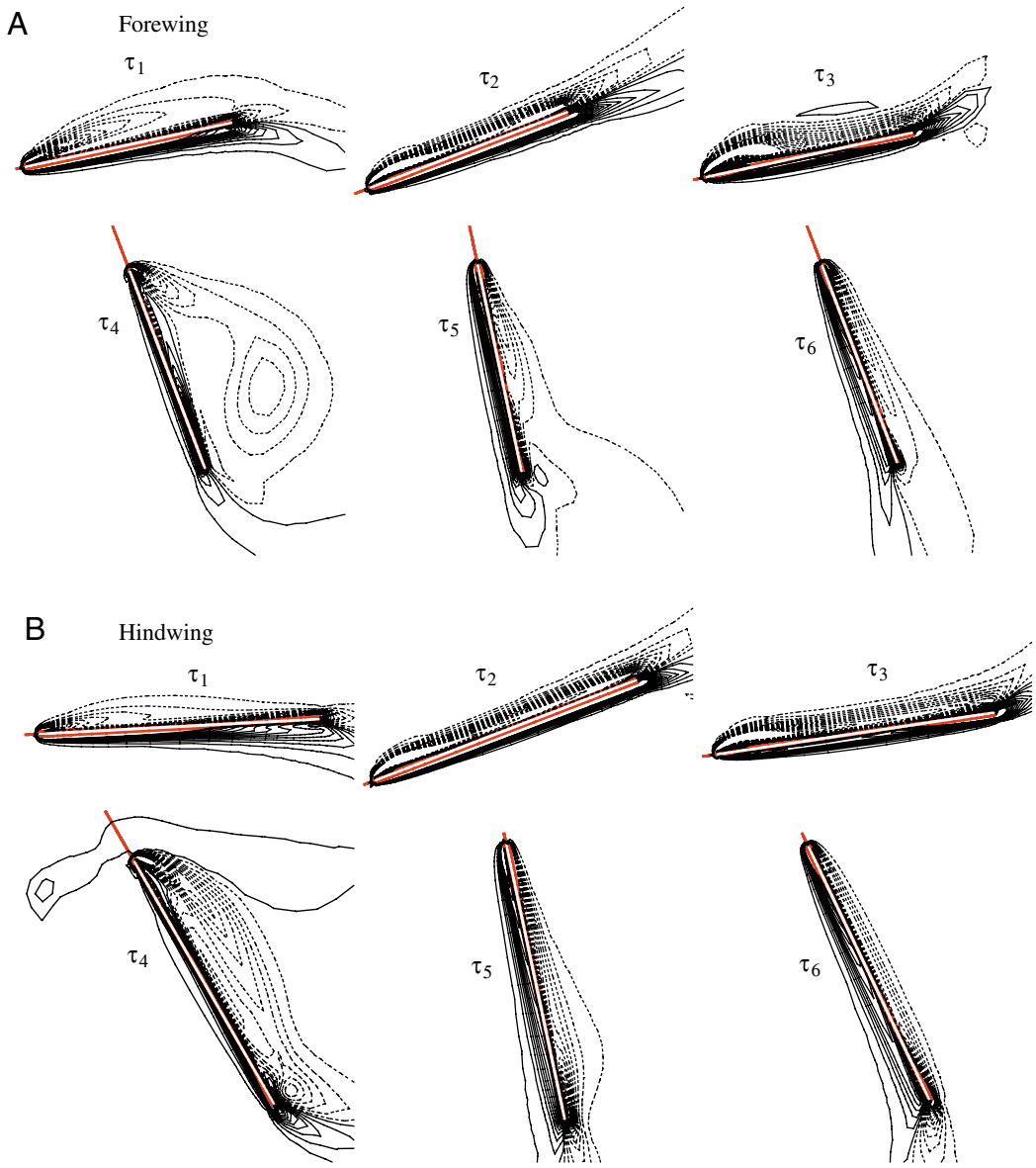

Fig. 14. Plot of spanwise component of vorticity at half-wing length at various time in a stroke cycle for the forewing (A) and the hindwing (B), at γ_d=60°, J=0.6 (α_d=31° and =50°). Solid and broken lines indicate positive and negative vorticity, respectively; the magnitude of non-dimensional vorticity at the outer contour is 1 and the contour internal is 3. γ_d, difference in phase angle between the hindwing and forewing; J, advance ratio; α_d and α_u, geometric angles of attack in the down- and upstrokes, respectively; τ, non-dimensional time.

defined in the conventional way; that is, the reference velocity used is the relative velocity of the wing; note that reference velocity used in the definition of the aerodynamic force coefficients in the proceeding sections is U, which is smaller than the relative velocity of the forewing or the hindwing in the case of forward flight). The dragonfly must use the separated flows with LEVs to generate the high aerodynamic force coefficients.

At high J, the relative velocity is contributed by both the flapping motion and the relatively high forward velocity and is relatively high. Thus, relatively low aerodynamic force coefficients are needed. The dragonfly does not need to use separated flows; instead, it uses attached flows. As an example,

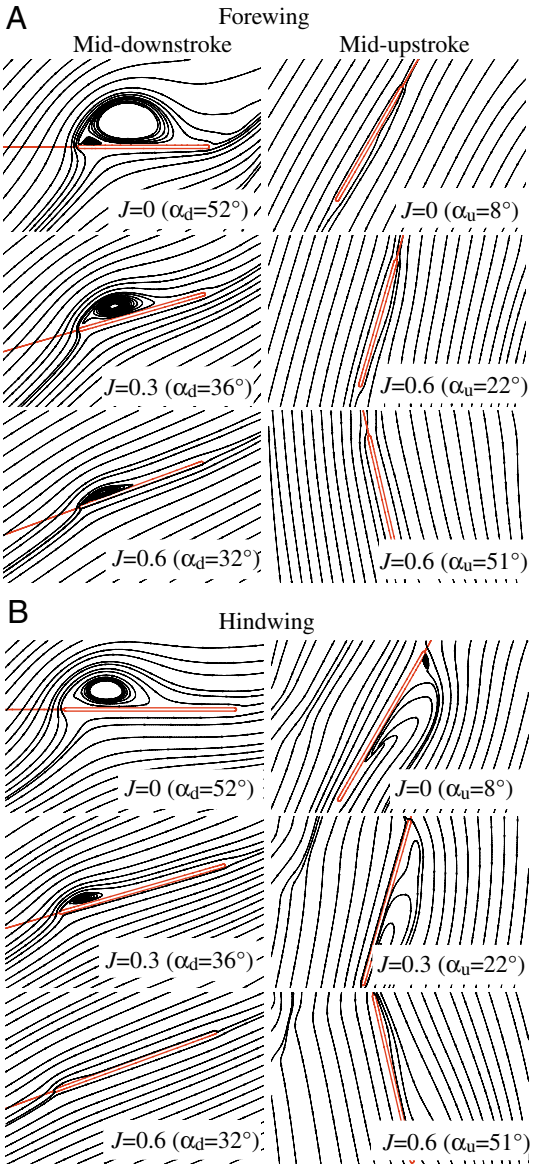

Fig. 15. Sectional streamline plots at half-wing length at the mid-downstroke and mid-upstroke of the forewing (A) and the hindwing (B) at various J (γ_d=180°). γ_d, difference in phase angle between the hindwing and forewing; J, advance ratio; α_d and α_u, geometric angles of attack in the down- and upstrokes, respectively.

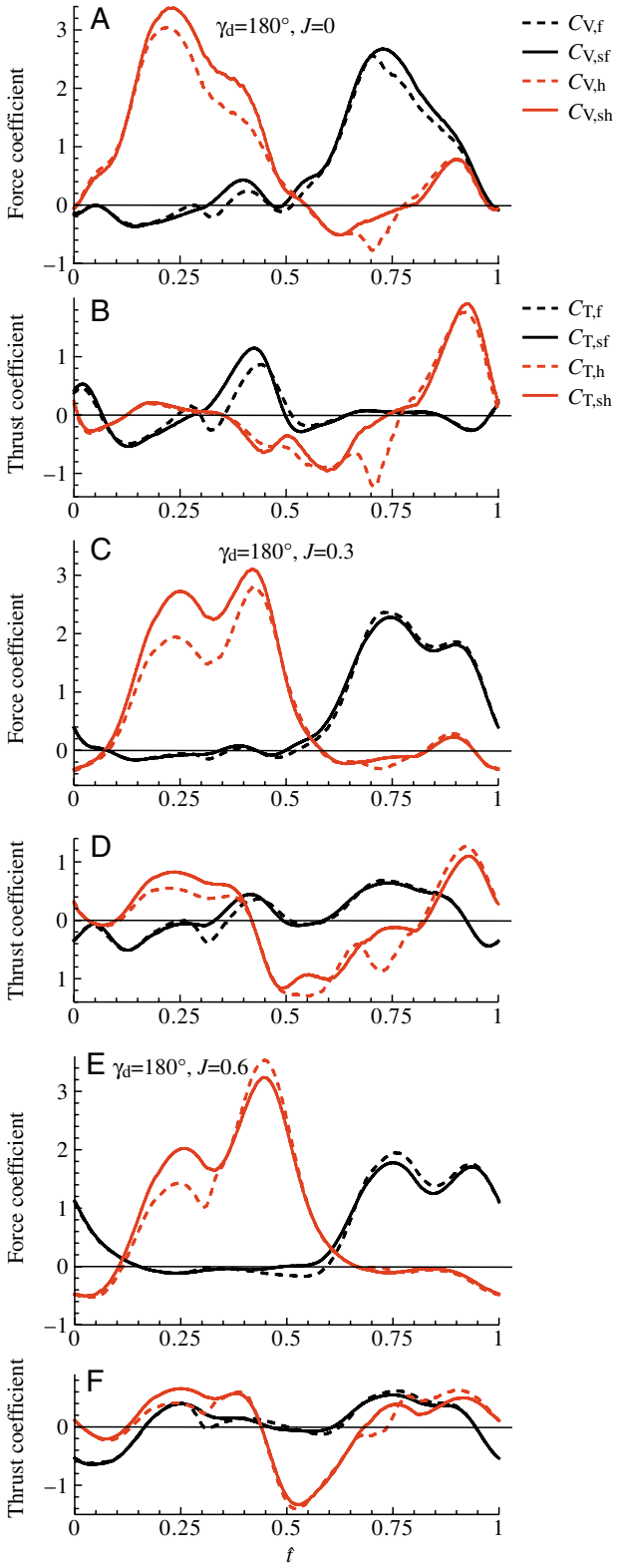

Fig. 16. Time courses of vertical force coefficients of forewing ($C_{V,f}$), single forewing ($C_{V,sf}$), hindwing ($C_{V,h}$) and single hindwing ($C_{V,sh}$) and thrust coefficients of the forewing ($C_{T,f}$), single forewing ($C_{T,sf}$), hindwing ($C_{T,h}$) and single hindwing ($C_{T,sh}$) in one cycle: (A,B) γ_d=180°, J=0; (C,D) γ_d=180°, J=0.3; (E,F) γ_d=180°, J=0.6. γ_d, difference in phase angle between the hindwing and forewing; J, advance ratio; $\hat{t}$, non-dimensional time.

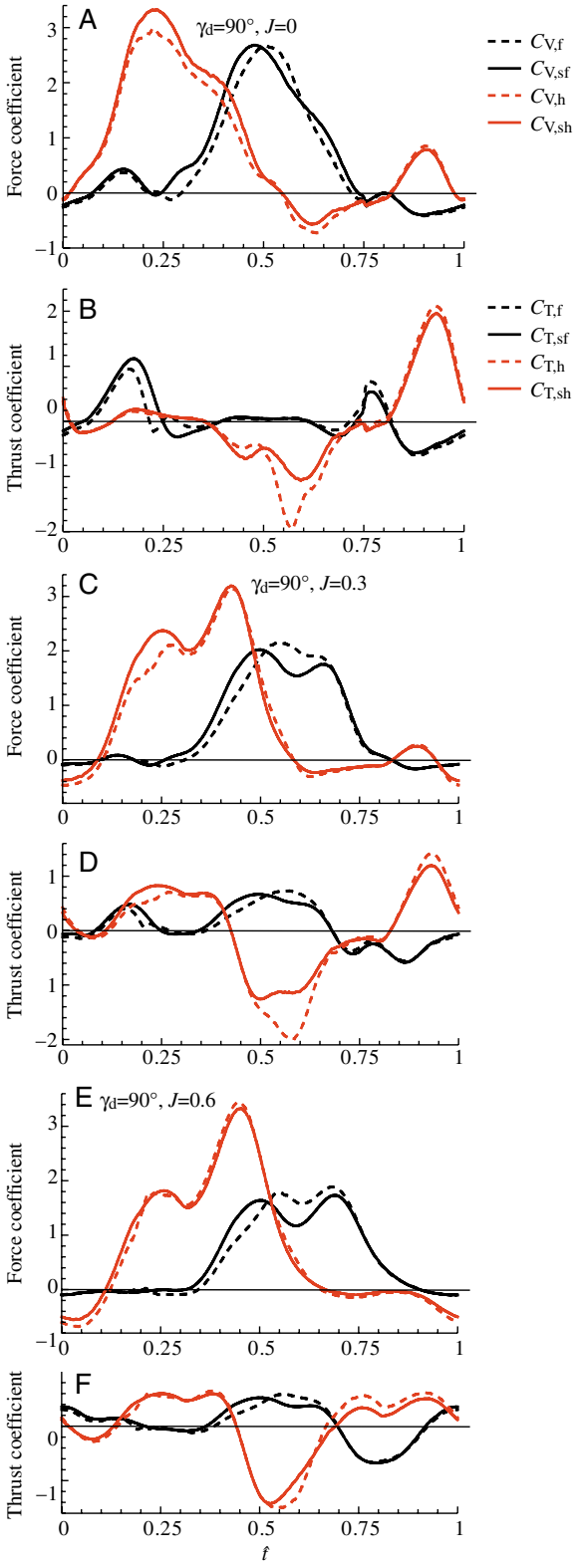

Fig. 17. Time courses of vertical force coefficients of forewing ($C_{V,f}$), single forewing ($C_{V,sf}$), hindwing ($C_{V,h}$) and single hindwing ($C_{V,sh}$) and thrust coefficients of the forewing ($C_{T,f}$), single forewing ($C_{T,sf}$), hindwing ($C_{T,h}$) and single hindwing ($C_{T,sh}$) in one cycle; (A,B) γ_d=90°, J=0; (C,D) γ_d=90°, J=0.3; (E,F) γ_d=90°, J=0.6. γ_d, difference in phase angle between the hindwing and forewing; J, advance ratio; $\hat{t}$, non-dimensional time.

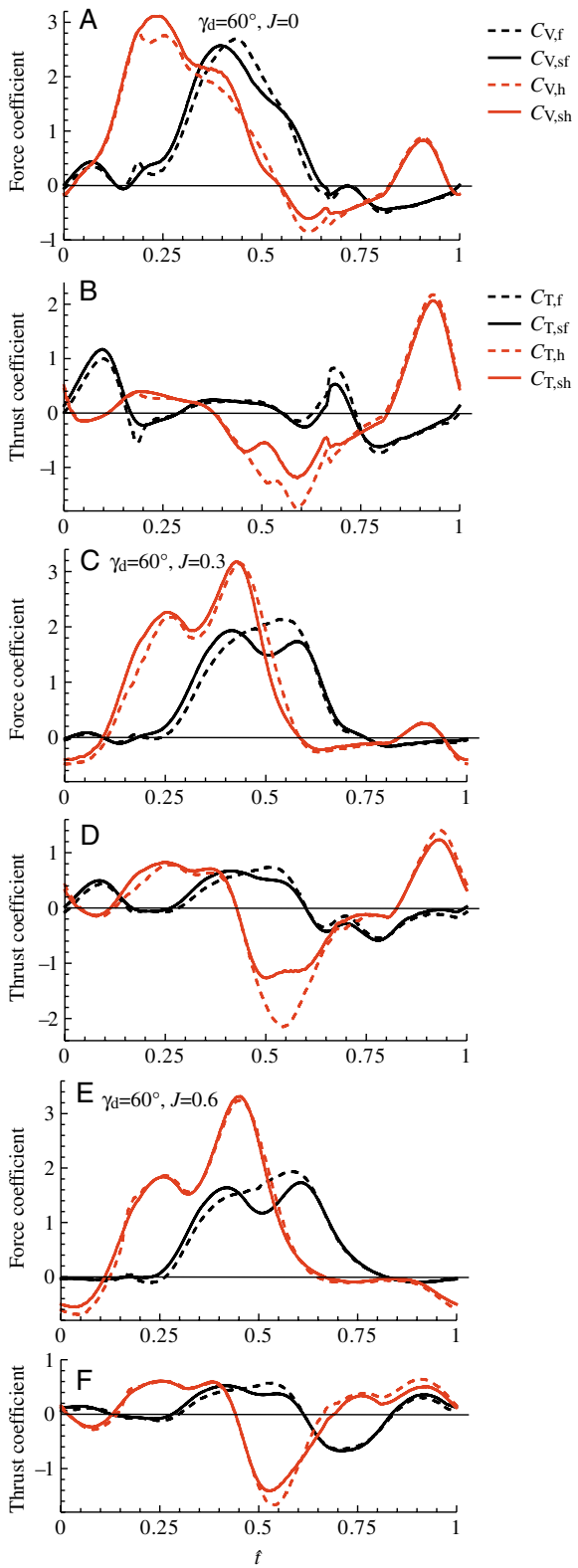

Fig. 18. Time courses of vertical force coefficients of forewing ($C_{V,f}$), single forewing ($C_{V,sf}$), hindwing ($C_{V,h}$) and single hindwing ($C_{V,sh}$) and thrust coefficients of the forewing ($C_{T,f}$), single forewing ($C_{T,sf}$), hindwing ($C_{T,h}$) and single hindwing ($C_{T,sh}$) in one cycle; (A,B) γ_d=60°, J=0; (C,D) γ_d=60°, J=0.3; (E,F) γ_d=60°, J=0.6. γ_d, difference in phase angle between the hindwing and forewing; J, advance ratio; $\hat{t}$, non-dimensional time.

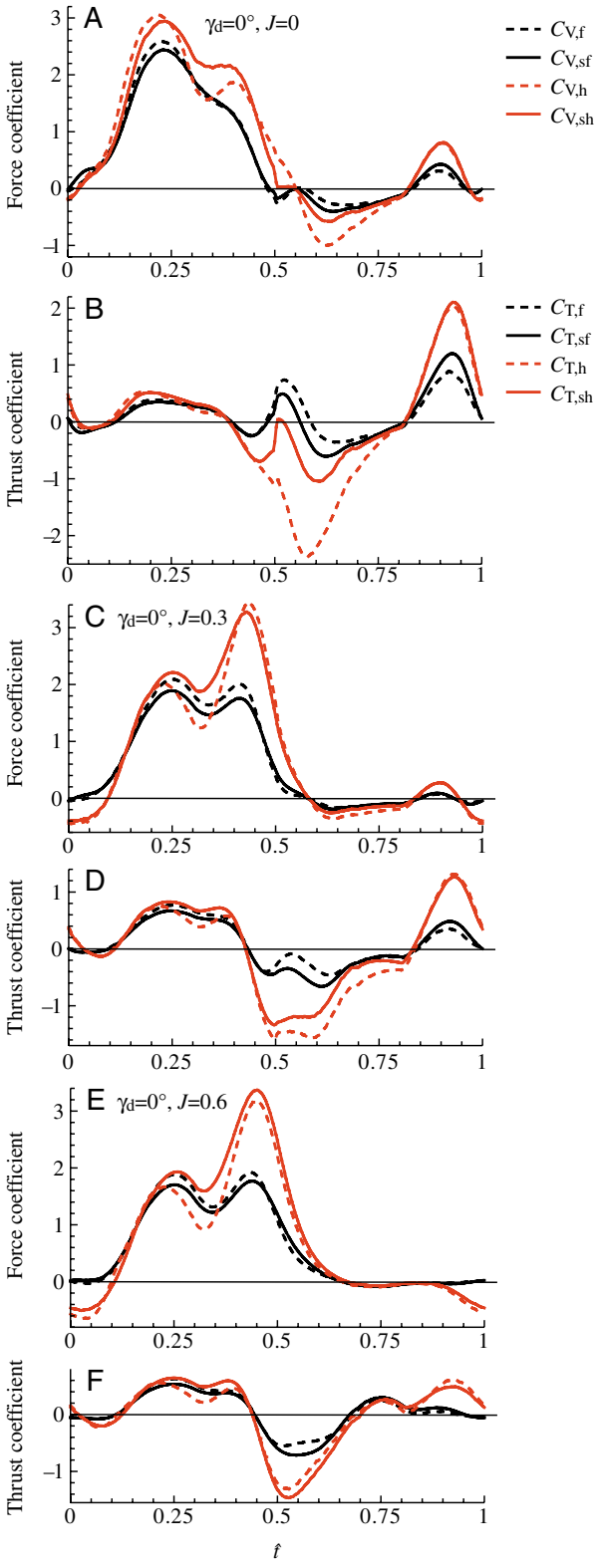

Fig. 19. Time courses of vertical force coefficients of forewing ($C_{V,f}$), single forewing ($C_{V,sf}$), hindwing ($C_{V,h}$) and single hindwing ($C_{V,sh}$) and thrust coefficients of the forewing ($C_{T,f}$), single forewing ($C_{T,sf}$), hindwing ($C_{T,h}$) and single hindwing ($C_{T,sh}$) in one cycle; (A,B) γ_d=0°, J=0; (C,D) γ_d=0°, J=0.3; (E,F) γ_d=0°, J=0.6. γ_d, difference in phase angle between the hindwing and forewing; J, advance ratio; $\hat{t}$, non-dimensional time.

Table 3. *The effects of forewing–hindwing interaction on mean vertical force and mean resultant force*

	$\Delta\hat{C}_V$ (%)			
J	γ_d=180°	γ_d=90°	γ_d=60°	γ_d=0°
0	–15 (–15.3)	–14.3 (–14.3)	–7.8 (–7.9)	–2.7 (–4.0)
0.15	–15 (–15.5)	–12.7 (–13.2)	–5.1 (–8.2)	–2.6 (–3.1)
0.30	–13.4 (–13.6)	–7.5 (–7.9)	–3.4 (–4.0)	–2.6 (–2.9)
0.45	–8.9 (–9.1)	–3.2 (–3.3)	0 (–0.6)	–5.9 (–6.0)
0.60	–5.6 (–5.7)	–1.6 (–1.5)	0 (–0.3)	–8.6 (–8.2)
0.75	–4.2 (–4.1)	–1.8 (–1.4)	–2.8 (–2.4)	–13.5 (–13.1)

J, advance ratio; γ_d, phase difference angle between fore- and hindwings; $\Delta\hat{C}_V$, percentage of increment in mean total vertical force coefficient due to interaction (negative number means interaction is detrimental). The numbers in parentheses are the corresponding results of the mean total resultant force coefficient.

we estimate the mean relative velocity of a section of the forewing (or hindwing) at a distance r_2 from the wing root at J=0.6. Using the diagram in Fig. 20, the relative velocity is estimated as 1.78U [U is the mean relative velocity of this section at hovering (J=0)]. The mean relative velocity is 1.78 times as large as that at hovering, and the vertical force coefficient needed would be about one-third of that needed for hovering. Therefore, at J=0.6, attached flows could produce the required aerodynamic force coefficients.

Comparison with flow visualization results of free-flying dragonflies

Recently, Thomas et al. (2004) presented flow visualization results for free-flying and tethered dragonflies. Some of their visualization tests were made for the dragonfly *Aeshna mixta* flying freely at V_∞=1.0 m s^{-1} (see, for example, fig. 6 of Thomas et al., 2004). Their results show that the dragonfly uses counter-stroking (γ_d=180°), with an LEV on the forewing downstroke and attached flow on the hindwing down- and upstrokes. The model dragonfly in the present study is

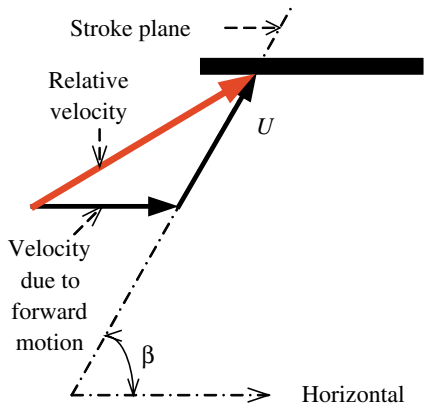

Fig. 20. Diagram used for computing the mean relative velocity of the section at r_2 from the wing root. β, stroke plane angle; r_2, radius of the second moment of wing area; U, velocity due to flapping.

modelled using the available morphological and kinematic data of the dragonfly *Aeshna juncea*, which is of the same genus as the dragonfly in the experiment. Moreover, in the flight of the model dragonfly, force-balance conditions are satisfied, and the flight could be a good approximation of the real flight. Therefore, we can make comparisons between the computed and experimental results. At U=0.3, V_∞ of the model dragonfly is 1.23 m s^{-1}, close to that in the experiment. Our results show that at this flight velocity there is a LEV on the forewing downstroke and the flows on the hindwing down- and upstrokes are approximately attached (Figs 10B, 15), in agreement with the flow visualization results of the free-flying dragonfly.

The above comparison is for an intermediate advance ratio. For high and very low advance ratios, there are also similarities between the visualizations of Thomas et al. (2004) and the simulation of the present study. Based on two available free flight sequences, Thomas et al. (2004) suggested (p. 4308) that at fast flight (high advance ratio), flows on the forewing and the hindwing were both attached; our results show that at J=0.6 (Figs 11, 14), the flows on both the forewing and the hindwing are approximately attached. At very low speed, they showed (video S2 in their supplementary material) that flows were separated on the hindwing as well as on the forewing; our simulation gives similar results (Figs 9, 12).

List of symbols

c	mean chord length of forewing
$C_{D,b}$	body-drag coefficient
$C_{d,f}$	drag coefficient of forewing
$C_{d,h}$	drag coefficient of hindwing
$C_{l,f}$	lift coefficient of forewing
$C_{l,h}$	lift coefficient of hindwing
$\overline{C}_T$	mean total thrust coefficient
C_T	total thrust coefficient
$C_{T,f}$	thrust coefficient of forewing
$C_{T,h}$	thrust coefficient of hindwing
$C_{T,sf}$	thrust coefficient of single forewing
$C_{T,sh}$	thrust coefficient of single hindwing
$\overline{C}_V$	mean total vertical force coefficient
C_V	total vertical force coefficient
$C_{V,f}$	vertical force coefficient of forewing
$C_{V,h}$	vertical force coefficient of hindwing
$C_{V,NI}$	total vertical force coefficient without interaction
$\overline{C}_{V,NI}$	mean total vertical force coefficient without interaction
$C_{V,sf}$	vertical force coefficient of single forewing
$C_{V,sh}$	vertical force coefficient of single hindwing
ΔC_V	percentage of increment in mean total vertical force coefficient due to forewing–hindwing interaction
$C_{V,W}$	mean vertical force required for balancing the weight
d_f	drag, forewing
d_h	drag, hindwing
J	advance ratio
l_f	lift, forewing
l_h	lift, hindwing
m	mass of the insect
n	flapping frequency
O	origin of the inertial frame of reference
r	radial position along wing length
R	wing length
r_2	radius of the second moment of wing area of forewing
Re	Reynolds number
S_f	area of one wing (forewing)
S_h	area of one wing (hindwing)
t	time
$\hat{t}$	non-dimensional parameter expressing time during a cycle ($\hat{t}$=0 at the start of the downstroke of the hindwing and $\hat{t}$=1 at the end of the following upstroke)
T	total thrust
T_f	thrust of forewing
T_h	thrust of hindwing
T_{sf}	thrust of single forewing
T_{sf}	thrust of single hindwing
U	reference velocity
u_t	translational velocity of a wing
u_t^+	non-dimensional translational velocity of a wing
$\overline{V}$	mean total vertical force
V	total vertical force
V_∞	free-stream velocity or flight velocity
V_f	vertical force of forewing
V_h	vertical force of hindwing
V_{NI}	vertical force without interaction
V_{sf}	vertical force of single forewing
V_{sh}	vertical force of single hindwing
X,Y,Z	coordinates in inertial frame of reference (Z in vertical direction)
$\dot{\alpha}$	angular velocity of flip rotation
$\dot{\alpha}^+$	non-dimensional angular velocity of flip rotation
$\dot{\alpha}_0{}^+$	a constant
α_d	geometrical angle of attack of downstroke
α_u	geometrical angle of attack of upstroke
β	stroke plane angle
γ	phase angle of the translation of a wing
γ_d	difference in phase angle between the hindwing and the forewing
$\dot{\phi}$	angular velocity of azimuthal rotation
ϕ	azimuthal or positional angle
$\overline{\phi}$	mean flapping angle
Φ	stroke amplitude
ν	kinematic viscosity of the air
ρ	density of fluid
τ	non-dimensional time
τ_c	period of one flapping cycle (non-dimensional)
τ_r	time when pitching rotation starts (non-dimensional)
$\Delta\tau_r$	duration of wing rotation or flip duration (non-dimensional)

We thank the two referees whose helpful comments and valuable suggestions greatly improved the quality of the paper. This research was supported by the National Natural Science Foundation of China (10232010, 10472008).

References

Alexander, D. E. (1986). Wing tunnel studies of turns by flying dragonflies. *J. Exp. Biol.* **122**, 81-98.

Azuma, A. and Watanabe, T. (1988). Flight performance of a dragonfly. *J. Exp. Biol.* **137**, 221-252.

Dickinson, M. H., Lehman, F. O. and Sane, S. P. (1999). Wing rotation and the aerodynamic basis of insect flight. *Science* **284**, 1954-1960.

Freymuth, P. (1990). Thrust generation by an airfoil in hover modes. *Exp. Fluids* **9**, 17-24.

Lan, S. L. and Sun, M. (2001a). Aerodynamic properties of a wing performing unsteady rotational motions at low Reynolds number. *Acta Mech.* **149**, 135-147.

Maybury, W. J. and Lahmann, F. (2004). The fluid dynamics of flight control by kinematic phase lag variation between two robotic insect wings. *J. Exp. Biol.* **207**, 4707-4726.

Norberg, R. A. (1972). The pterostigma of insect wings and inertial regulator of wing pitch. *J. Comp. Physiol*. **81**, 9-22.

Norberg, R. A. (1975). Hovering flight of the dragonfly *Aeschna juncea* L., kinematics and aerodynamics. In *Swimming and Flying in Nature* (ed. T. Y. Wu, C. J. Brokaw and C. Brennen), pp. 763-781. New York: Plenum Press.

Reavis, M. A. and Luttges, M. W. (1988). Aerodynamic forces produced by a dragonfly. *AIAA* Paper 88-0330.

Rogers, S. E. and Kwak, D. (1990). Upwind Differencing scheme for the time-accurate incompressible Navier–Stokes equations. *AIAA J.* **28**, 253-262.

Rogers, S. E., Kwak, D. and Kiris, C. (1991). Steady and unsteady solutions of the incompressible Navier–Stokes equations. *AIAA J.* **29**, 603-610.

Rogers, S. E. and Pulliam, T. H. (1994). Accuracy enhancements for overset grids using a defect correction approach. *AIAA* Paper 94-0523.

Saharon, D. and Luttges, M. (1988). Visualization of unsteady separated flow produced by mechanically driven dragonfly wing kinematics model. *AIAA* Paper 88-0569.

Saharon, D. and Luttges, M. (1989). Dragonfly unsteady aerodynamics: the role of the wing phase relations in controlling the produced flows. *AIAA* Paper 89-0832.

Somps, C. and Luttges, M. (1985). Dragonfly flight: novel uses of unsteady separation flows. *Science* **28**, 1326-1328.

Sun, M. and Lan, S. L. (2004). A computational study of the aerodynamic forces and power requirements of dragonfly (*Aeshna juncea*) hovering. *J. Exp. Biol.* **207**, 1887-1901.

Sun, M. and Tang, J. (2002). Unsteady aerodynamic force generation by a model fruit fly wing in flapping motion. *J. Exp. Biol.* **205**, 55-70.

Thomas, A. L. R., Taylor, G. K., Srygley, R. B., Nudds, R. L. and Bomphrey, R. J. (2004). Dragonfly flight: free-flight and tethered flow visualizations reveal a diverse array of unsteady lift-generating mechanisms, controlled primarily via angle of attack. *J. Exp. Biol.* **207**, 4299-4323.

Wakeling, J. M. and Ellington, C. P. (1997a). Dragonfly flight (1). Gliding flight and steady-state aerodynamic forces. *J. Exp. Biol.* **200**, 543-556.

Wakeling, J. M. and Ellington, C. P. (1997b). Dragonfly flight (2). Velocities, accelerations and kinematics of flapping flight. *J. Exp. Biol.* **200**, 557-582.

Wakeling, J. M. and Ellington, C. P. (1997c). Dragonfly flight (3). Quasi-steady lift and power requirements. *J. Exp. Biol.* **200**, 583-600.

Wang, H., Zeng, L. J., Liu, H. and Yin, C. Y. (2003). Measuring wing kinematics, flight trajectory and body attitude during forward flight and turning maneuvers in dragonflies. *J. Exp. Biol.* **206**, 745-757.

Wang, Z. J. (2000). Two dimensional mechanism for insect hovering. *Phys. Rev. Lett.* **85**, 2216-2219.

Wang, Z. J. (2004). The role of drag in insect hovering. *J. Exp. Biol.* **207**, 4147-4155.